HHS Public Access

Author manuscript

Sci Immunol. Author manuscript; available in PMC 2022 June 24.

Published in final edited form as:

Sci Immunol. 2021 December 24; 6(66): eabf2489. doi:10.1126/sciimmunol.abf2489.

Mitochondrial C5aR1 activity in macrophages controls IL-1β production underlying sterile inflammation

Nathalie Niyonzima[1], **Jubayer Rahman**[2], **Natalia Kunz**[2], **Erin E. West**[2], **Tilo Freiwald**[3], **Jigar V. Desai**[4], **Nicolas S. Merle**[2], **Alexandre Gidon**[1], **Bjørnar Sporsheim**[1,5], **Michail S. Lionakis**[4], **Kristin Evensen**[6], **Beate Lindberg**[7], **Karolina Skagen**[8], **Mona Skjelland**[8,9], **Parul Singh**[2], **Markus Haug**[1,10], **Marieta M. Ruseva**[11], **Martin Kolev**[11], **Jack Bibby**[2], **Olivia Marshall**[12], **Brett O'Brien**[12], **Nigel Deeks**[12], **Behdad Afzali**[3], **Richard J. Clark**[13], **Trent M. Woodruff**[13], **Milton Pryor**[14], **Zhi-Hong Yang**[14], **Alan T. Remaley**[14], **Tom E. Mollnes**[1,15,16,17], **Stephen M. Hewitt**[18], **Bingyu Yan**[19], **Majid Kazemian**[19], **Máté G. Kiss**[20,21], **Christoph J. Binder**[20,21], **Bente Halvorsen**[8,22], **Terje Espevik**[1,10,*], **Claudia Kemper**[2,23,*]

[1]Center of Molecular Inflammation Research (CEMIR), Department of Cancer Research and Molecular Medicine, Norwegian University of Science and Technology (NTNU), Trondheim, Norway,

[2]Complement and Inflammation Research Section (CIRS), National Heart, Lung, and Blood Institute (NHLBI), National Institutes of Health (NIH), Bethesda, MD 20892, USA,

[3]Immunoregulation Section, Kidney Diseases Branch, National Institute of Diabetes and Digestive and Kidney Diseases (NIDDK), NIH, Bethesda, MD 20892, USA,

[4]Fungal Pathogenesis Section, Laboratory of Clinical Immunology and Microbiology, National Institute of Allergy and Infectious Disease, National Institutes of Health, Bethesda MD 20892, USA.

[5]Central Administration, St. Olavs Hospital, The University Hospital in Trondheim, Trondheim, Norway,

[6]Department of Neurology, Vestre Viken, Drammen Hospital, Drammen, Norway.

[7]Department of Cardiothoracic Surgery, Oslo University Hospital, Rikshospitalet, Oslo, Norway,

[8]Department of Neurology, Oslo University Hospital, Rikshospitalet, Oslo, Norway,

[9]Institute of Clinical Medicine, University of Oslo, Oslo, Norway,

[10]The Central Norway Regional Health Authority, St. Olavs Hospital HF, Norway

[11]BG2, Adaptive Immunity Research Unit, GlaxoSmithKline, Stevenage, UK,

[*]These authors contributed equally to the work. Corresponding authors: terje.espevik@ntnu.no or Claudia.kemper@nih.gov.

Author contributions:

N.N., T.E., and C.K. conceived the project, designed and/or performed experiments, analyzed and interpreted the data and wrote the manuscript; J.R., N.K., E.E.W, T.F., J.V.D., N.S.M., A.G., B.A., M.P, Z.-H.Y., B.S., P.S., M.H., and M.G.K. performed experiments and analyzed data; S.M.H. performed the kidney pathology analyses; K.E., B.L., K.S., M.S., and B.H., designed the experiments relating to the patient data, selected the patients, and isolated and processed the carotid plaques. J.B., M.K., B.A., and B.Y. performed the computational analyses. T.M.W. and R.J.C. generated and provided the C5aR antagonists and M.K. and M.M.R. developed the cpFBinh. O.M., B.O'B., and N.D. performed the mass spectrometry analysis defining the cell-permeability of JPE1375. M.S.L, T.M.W., T.E.M., A.T.R., C.F.B., T.E., and C.K. designed experiments and critically revised and edited the manuscript.

Competing interests: All other authors declare no competing interests.

[12]Discovery DMPK Bioanalysis Unit, GlaxoSmithKline, Stevenage, UK,

[13]School of Biomedical Sciences, The University of Queensland, Queensland, Australia,

[14]Lipoprotein Metabolism Section, Cardiopulmonary Branch, NHLBI, NIH, Bethesda, MD 20892, USA,

[15]Department of Immunology, Oslo University Hospital Rikshospitalet, and University of Oslo, Oslo, Norway,

[16]Research Laboratory, Nordland Hospital, Bodø, Norway,

[17]K.G. Jebsen TREC, Institute of Clinical Medicine, University of Tromsø, Tromsø, Norway,

[18]Laboratory of Pathology, National Cancer Institute (NCI), NIH, Bethesda, MD 20892, USA,

[19]Departments of Biochemistry and Computer Science, Purdue University, West Lafayette, IN 47907, USA,

[20]Department of Laboratory Medicine, Medical University of Vienna, Vienna, Austria.

[21]CeMM Research Center for Molecular Medicine of the Austrian Academy of Sciences, Vienna, Austria,

[22]Research Institute of Internal Medicine, Oslo University Hospital Rikshospitalet, Oslo, Norway,

[23]Institute for Systemic Inflammation Research, University of Lübeck, Lübeck, Germany.

Abstract

While serum-circulating complement destroys invading pathogens, intracellularly active complement, termed the ‘complosome’, functions as a vital orchestrator of cell-metabolic events underlying T cell effector responses. Whether intracellular complement is also non-redundant for the activity of myeloid immune cells is currently unknown. Here, we show that monocytes and macrophages constitutively express complement component (C) 5 and generate autocrine C5a via formation of an intracellular C5 convertase. Cholesterol crystal-sensing by macrophages induced C5aR1 signaling on mitochondrial membranes, which shifted ATP production via reverse electron chain flux towards reactive oxygen species (ROS) generation and anaerobic glycolysis to favor IL-1β production, both at the transcriptional level and processing of pro-IL-1β. Consequently, atherosclerosis-prone mice lacking macrophage-specific *C5ar1* had ameliorated cardiovascular disease on a high-cholesterol diet. Conversely, inflammatory gene signatures and IL-1β produced by cells in unstable atherosclerotic plaques of patients were normalized by a specific cell-permeable C5aR1 antagonist. Deficiency of the macrophage cell autonomous C5 system also protected mice from crystal nephropathy mediated by folic acid. These data demonstrate the unexpected intracellular formation of a C5 convertase and identify C5aR1 as a direct modulator of mitochondrial function and inflammatory output from myeloid cells. Together, these findings suggest that the complosome is a contributor to the biologic processes underlying sterile inflammation and indicate that targeting this system could be beneficial in macrophage-dependent diseases, such as atherosclerosis.

ONE SENTENCE SUMMARY

Mitochondrial C5aR1 signaling is required for pro-inflammatory macrophage activity during crystal-induced sterile inflammation.

INTRODUCTION

The liver-derived and plasma-circulating complement system is a key member of the host's repertoire of pathogen- and damage-associated molecular patterns (PAMP and DAMP) sensors. Pathogen-sensing in blood triggers activation of C3 into C3a and C3b and of C5 into C5a and C5b, by C3 and C5 convertases, respectively. These complement activation fragments together mediate opsonization and removal of invading microbes, mobilization of immune cells, and induction of a general inflammatory reaction. Recent work, however, has led to the unexpected discovery of a cell-autonomous, intracellularly active, complement system, termed the complosome.

The complosome is central to the regulation of the basic metabolic pathways underlying normal function of immune cells. For example, the continuous cell-intrinsic expression and activation of C3 sustains homeostatic survival of circulating human T cells via tonic mammalian target of rapamycin (mTOR) activation (1). Cell-autonomous C3 activation fragments generated upon T cell activation also induce the bioenergetic adaptations required for the induction of $CD4^+$ T helper (Th) 1 and $CD8^+$ cytotoxic T cell (CTL) responses, by enabling nutrient influx, mammalian target of rapamycin complex 1 (mTORC1) activation, glycolysis, oxidative phosphorylation (OXPHOS) and reactive oxygen species (ROS) production (2–6). Similarly, human monocytes rely on intrinsic C3a activity for their production of IL-1β during infections (7). Thus, cell-intrinsic, intracellular, complement C3 activity is an integral part of normal human immune cell responses, while hypo- or hyper-active complosome activity are, in turn, associated with recurrent infections or autoimmune diseases, respectively (1, 8–10). We have recently shown that T cells also express C5 and that intracellular C5aR1 signaling after during T cell receptor (TCR) stimulation initiates the ROS-mediated assembly of a T cell-intrinsic canonical NACHT, LRR and PYD domains-containing protein 3 (NLRP3) inflammasome, which enhances secretion of mature (IL)-1β and potentiates the magnitude of the Th1 response (11). It is currently unknown whether myeloid cells also harbor a C5 system and/or recruit intracellular C5aR1 for normal function following danger-sensing.

Sterile inflammation, that is inflammation caused by DAMPs in the absence of infection, critically depends on leukocyte function and contributes to a broad range of human pathologies, including ischemic reperfusion injury, arthritic diseases, and atherosclerotic cardiovascular disease (ACVD) (12). ACVD is a leading cause of death worldwide and cardinal features of this condition include cholesterol accumulation and precipitation into crystalline cholesterol (CC) in arterial walls, events that trigger chronic (local) inflammation, and ultimately the formation of atherosclerotic plaques, causing vaso-occlusive diseases. Patrolling monocytes that detect and ingest CC present in early atherosclerotic lesions (13) and monocyte-derived pro-inflammatory foam cells residing within the atherosclerotic lesions play pivotal roles in the induction and progression of ACVD via NLRP3-dependent production of IL-1β (14, 15). As CC in circulation can activate serum complement (16,

17), we hypothesized that DAMP-sensing of phagocytes following CC uptake involves the complosome. We focused on the intracellular 'C5 system' as its activity is unexplored in myeloid cells.

Here, we report that human monocytes and macrophages continuously synthesized C5 and generated C5a intracellularly via a cell-intrinsic intracellular C5 convertase. Furthermore, myeloid cell mitochondria express C5aR1 (mtC5aR1) and engagement of mtC5aR1 was required for optimal IL-1β production by monocytes and macrophages upon crystal-sensing. Mechanistically, mtC5aR1 shifted adenosine triphosphate (ATP) production by these organelles, via reverse electron chain flux towards ROS production and aerobic glycolysis, to favor *IL1B* gene transcription and production of mature IL-1β. The biological significance of mtC5aR1 activity in the induction of crystal-triggered sterile inflammation was underpinned by two findings: mice lacking *C5ar1* expression only in myeloid cells developed less severe disease in models of folic acid-induced kidney injury and in Western diet-precipitated ACVD. Further, exposure of cells within carotid plaques of patients with atherosclerosis to a cell-permeable C5aR1 antagonist reduced their IL-1β secretion and inflammatory gene signatures. Overall, these data identify the anaphylatoxin receptor C5aR1 as a direct modulator of myeloid cell mitochondrial function and support a key role for the complosome in the processes underlying non-resolving, sterile inflammation.

RESULTS

Intracellular C5aR1 supports IL-1β production in cholesterol crystal-sensing macrophages

To examine the activity of the intracellular C5 in myeloid cells, we isolated human monocytes from blood and stained them for C5 complosome components. We detected substantial intracellular C5 together with processed C5a stores, and expression of both the classical C5aR1 and the alternative C5aR2 both intracellularly and on the cell surface (Fig. 1A). T and B cells in culture can endocytose C3(H_2O) (18). The presence of *C5* mRNA (Fig. 1B), as well as C5 protein in the Golgi apparatus (Fig. 1C, and fig. S1A), however, supported cell-intrinsic generation of C5 in monocytes. We noticed that C5a was excluded from the Golgi apparatus (Fig. 1C, and fig. S1A), indicating that intracellular C5 is activated to C5a in a post-Golgi compartment.

To study the role of the C5 complosome during monocyte crystal-sensing, we blocked C5a receptor function during *in vitro* monocyte culture with LPS and/or CC using well-established, specific inhibitors of surface-expressed C5a receptors: the C5aR2 agonist peptide P32 (19) or the C5aR1 and C5aR2 double-antagonist A8Δ71–73 (20). Neither treatment had a significant effect on IL-1β secretion by monocytes stimulated with LPS and/or CC (Fig. 1D), whereas inhibition of the NLRP3 inflammasome by the inhibitor MCC950 reduced IL-1β secretion (Fig. 1E). We next blocked C5aR1 intracellularly using the C5aR1 inhibitor JPE1375, which displays higher cell-permeability compared to PMX53 (fig. S1B). JPE1375 reduced IL-1β secretion by ~50% during monocyte stimulation with LPS+CC (Fig. 1F). This effect was specific to IL-1β as JPE1375 had no impact on the production of tumor necrosis factor (TNF) or IL-10 (Fig. S1C). While exposure of human monocytes to increasing amounts of LPS or CC induced, as expected, a proportional increase in cell death (fig. S1D), the *in vitro* priming and CC activation conditions used

here did not affect cell viability and neither did addition of PMX53 or JPE1375 to cultures (fig. S1E).

To next determine if and how priming and/or CC sensing modulates the C5 system, we measured mRNA and protein levels of C5 components after monocyte stimulation. *C5AR1* transcription and protein expression increased > 2-fold upon CC and LPS+CC exposure, while *C5* and *C5aR2* transcription and protein concentrations remained largely unchanged across activation conditions. We noticed, however, that CC-sensing, with and without LPS-priming, augmented intracellular C5a generation and C5aR1 protein expression (fig. S1F and G). Moreover, while intracellular C5a pools and intracellular C5aR1 occupied largely distinct subcellular locations in resting monocytes, LPS+CC activation induced visibly increased colocalization of this receptor-ligand pair (Fig. 1G). We also noted colocalization between C5aR1 and NLRP3 in resting and activated monocytes (fig. S1H), although the implication of this finding is currently unclear. Together, these findings indicate that CC-sensing in monocytes mobilizes and engages the C5 complosome and supports IL-1β production.

We next assessed if our observations extended to macrophages as those represent the disease-driving cells in atherosclerotic lesions and other contexts of sterile inflammation. Indeed, human monocyte-derived macrophages (hMDM) also contained C5 and C5a stores, expressed the C5aRs in a pattern comparable to monocytes (fig. S1I), and displayed ~ 50% reduction in IL-1β secretion after LPS+CC activation upon selective intracellular C5aR1 blockage, without an effect on cell viability (Fig. 1H, and fig. S1J). Importantly, when LPS-primed hMDM were exposed to monosodium urate (MSU) crystals, which generally evoke a similar NLRP3-dependent IL-1β response, we also observed a significant decrease of IL-1β secretion in the presence of the cell-permeable C5aR1 inhibitor (Fig. 1H). These data indicate that intracellular C5aR1 activation may be a general feature during crystal-sensing in human myeloid cells.

We next probed whether the C5 complosome induces caspase-8 activation, because this can drive IL-1β secretion (21, 22). Exposure of hMDMs to *E.coli* induced caspase-8 activation whereas LPS priming and crystal-sensing did not (Fig. 1I), suggesting that C5aR1 drives IL-1β generation independently of caspase-8. In line with the inhibitor-generated data, knock-down of C5aR1 or C5 by siRNA technique in hMDM (fig. S1K) diminished mature IL-1β secretion (Fig. 1J) without impacting TNF or IL-10 production or cell viability (fig. S1L and M) in LPS+CC-stimulated macrophages. IL-1β production in response to the soluble inflammasome activator, nigericin, was also dependent on intracellular C5aR1 (Fig. 1K and L, and fig. S1N and O). Knock-down of either *C5* or *C5AR1* reduced both pro-IL-1β and mature IL-1β secretion (Fig. 1K, and fig. S1N and O) and *IL1B* mRNA generation (Fig. 1L) by crystal-activated cells. Thus, inhibition of C5 receptor engagement also impairs *IL1B* gene transcription (23). Importantly, under all activation conditions assessed, expression of genes encoding key NLRP3 inflammasome components, such as *NLRP3* and *ASC*, or the major NLRP3 inflammasome target, *CASP1*, was not changed (fig. S1P). However, higher doses of LPS augmented, as expected, *NLRP3* gene expression (fig. S1Q).

Interestingly, the effects of C5aR1 blockade on *in vitro*-differentiated human M1 and M2 macrophages upon LPS activation was different from those observed in monocytes and non-differentiated macrophages (fig. S1R and S). Production of IL-1β by M1 macrophages was refractory to C5aR1 inhibition, while the addition of JPE1375, but not PMX53, reduced their IL-10 secretion significantly. In M2 macrophages, on the other hand, all inhibitors reduced IL-1β and IL-6 secretion, with a strong trend to higher IL-10 production (fig. S1S). Together these data support the requirement for intracellular C5aR1 signalling in human monocytes and non-differentiated macrophages for normal *IL1B* transcription and subsequent processing of pro-IL-1β into the mature form by the NLRP3 inflammasome during DAMP (crystal)-sensing.

An intracellular C5 convertase drives C5a generation within CC-sensing monocytes

We next investigated the mechanism of C5 processing in myeloid cells. As human monocytes and macrophages express intrinsic C3 at steady state (7), we probed monocytes for the presence of mRNAs encoding *CFD* and/or *CFB*, which together would enable assembly of complement alternative pathway C3 (C3bBb) and C5 (C3bBbC3b) convertases. Freshly isolated monocytes expressed *CFD* and *CFB* at low levels and LPS priming significantly induced *CFB* (but not *CFD*) levels (Fig. 2A). Moreover, by double-staining with antibodies against C3b and the Bb neo-epitope (which denotes Factor B activation and thus convertase formation) we observed not only the presence of both C3b and cleaved Bb but also their colocalization in resting cells (Fig. 2B) and increased generation of C3/C5 convertase formation in primed CC-sensing monocytes (Fig. 2B). Multiple cell plane (z-stack) analyses confirmed the presence of C3bBb and/or C3bBbC3b complexes within the cell's interior (Fig. 2B). FACS analyses of resting and CC-activated, permeabilized or non-permeabilized, monocytes indicated that the majority of C5 convertases formed under the cell membrane, but that a proportion of convertases also localized to the monocyte cell surface (Fig. 2C and D). It is currently not possible to discriminate between formation of C3 vs. C5 convertases as both are composed of the same proteins assembled in different proportions. Western blot analyses of non-activated and CC -ctivated monocytes further confirmed the generation of the active Bb fragment by monocytes (Fig. 2E) and of FD protein (we were unable to determine whether cells contained the pro-form and/or the processed form of FD (24)) (Fig. 2F). Western blot analyses of subcellular fractions of resting human monocytes confirmed co-localization of C3b, Bb, and FD with the cell membrane (fig. S2A). Surprisingly, however, we also observed the presence of C3b, FB, Bb, and FD on mitochondria and other, not further defined, organelles (fig. S2A). The reduction of *FB* expression (Fig. 2G, **upper panel**) by siRNA led to a proportional decrease in IL-1β secretion by CC-exposed monocytes (Fig. 2G, **lower panel**) but did not reduce TNF generation (fig. S2B), in line with our observation that intracellular C5a specifically drives IL-1β production.

We next assessed the impact of a newly developed human FB inhibitor (cpFBinh) (25) on the monocyte cell-intrinsic C5 system. This FB inhibitor is highly cell-permeable (25) and hence potently inhibits both extra- and intracellular FB activity. To simplify the experimental set-up, we utilized high (100 ng/ml) LPS activation as strong toll-like receptor (TLR) 4 engagement drives both FB expression and IL-1β production. Activation of human

monocytes in the presence of cpFBinh indeed reduced intracellular C5a generation by high LPS-stimulated monocytes (Fig. 2H), which led to a concurrent decrease in their IL-1β production (Fig. 2I). The addition of an antibody to FB that inhibits FB-driven convertase formation only on the cell surface had a limited effect on intracellular C5a generation and IL-1β production (Fig. 2H and I). Incubation of LPS-activated monocytes with the C5aR1 inhibitor JPE1375 in the presence of the cpFBinh did not further reduce IL-1β production (fig. S2C). Together, these data support that human monocytes harbor a fully cell-autonomous C5 activation system. They also indicate the requirement for intracellular FB and C5 convertase activity to enable C5aR1 engagement for IL-1β production in DAMP-sensing human monocytes. Although human T cells require strictly cell-intrinsic C3 activation for IFN-γ production, they can source serum C3(H_2O) to modulate their IL-6 secretion in *in vitro* cultures (18). We found that neither addition of serum-purified C5(H_2O) (26, 27) nor C5a rescued cpFBi-mediated reduction in IL-1β production by stimulated monocytes *in vitro* (Fig. 2J), indicating that cell-autonomous C5a is likely required for optimal monocyte IL-1β production.

As monocytes can express a substantial range of complement proteins (7, 28), we explored if they may also engage components of the classical complement pathway. We noted *C4* and *C2* gene transcription as well as C4 and C2 protein expression in resting monocytes. Further, CC-sensing increased C4 protein expression (fig. S2D and E). Western blot analyses of resting and activated human monocytes confirmed that C4 and C2 were present mostly in their processed active forms as C4b and C2b, respectively (fig. S2F). Also, and similarly to C3b, C4b was predominantly intracellularly localized, while a relatively large proportion of C2b was present on the cell surface (fig. S2G and H). These observations suggest that monocytes may also support formation of intracellular classical pathway C3 and C5 convertases (C4bC2b and C4bC2bC3b), which warrants further exploration.

Together, these data demonstrate the intracellular formation of the central serum complement activation hubs, the C3/C5 convertases, in human monocytes and suggest that intracellular inhibition of the alternative pathway C3/C5 convertase formation may be a means to modulate IL-1β production by myeloid cells during sterile inflammation.

Mitochondrial C5aR1 controls ETC flux and mitochondrial dynamics

We next examined the localization and function of intracellular C5aR1 in monocytes. Western blots of sub-cellular fractions from resting human monocytes confirmed the presence of C5aR1 in the plasma membrane, the cytoplasm, mitochondria and other organelles, including lysosomes (fig. S3A and B). Because of our previous finding that intracellular C5aR1 in T cells augments ROS production during Th1 induction (11), we hypothesized that mitochondrial C5aR1 may impact mitochondrial activity, the principal source of ROS production in mammalian cells. C5aR1 was expressed on mitochondria in resting monocytes, specifically the outer mitochondrial membrane, as evidenced by co-localization with both a mitochondrial stain (Fig. 3A) and with TOM20 (Fig. 3B). This was confirmed by C5aR1 Immunogold staining and electron microscopy analyses of non-activated THP-1 cells, a human monocytic cell line (fig. S3C). We also observed colocalization of C5a with mitochondrial-expressed C5aR1 (mtC5aR1) (fig.

S3D), indicating that C5a is targeted to mtC5aR1 and could exert biological effects on mitochondria.

To probe whether mtC5aR1 can respond to ligand activation, isolated mitochondria were exposed to increasing amounts of serum-purified C5a ranging from 5 to 50 ng/ml (C5a amounts commonly found in circulation range from approximately 20 – 150 ng/ml). To obtain sufficient pure mitochondria, we utilized non-activated THP-1 cells. High purity of mitochondria in isolated sub-cellular fractions was confirmed by the absence of Ras-related protein Rab-11A (RAB11) and tubulin (fig. S3E). Addition of C5a to mitochondria evoked ROS production, a measure of mitochondrial activity, in a dose-dependent manner, and in a classic bell-shaped response profile characteristic of C5aR signaling elsewhere (Fig. 3C) (29). Pre-incubation of mitochondria with the C5aR1 antagonist JPE1375 or PMX53 or with pertussis toxin (which blocks G protein-coupled receptor (GPCR) signaling) blocked C5a-driven ROS production (Fig. 3D, and fig. S3F). Collectively, these data indicate that mitochondria express a functional C5aR1 that responds to specific C5a ligand engagement and induces ROS production via G protein coupling.

We next assessed the downstream signaling pathway(s) recruited by liganded mtC5aR1 in monocytes and macrophages. GPCR signaling, including that of C5aR1, has been studied traditionally with a focus on plasma membrane-embedded receptors. Nevertheless, GPCRs are also observed in cellular sub-compartments (30–32), where they can engage canonical signal transduction (33). In most cells, G-protein signaling coupled to plasma membrane-expressed C5aR1 recruits the ERK- MAPK signalosome and modulates levels of the second messenger cyclic adenosine 3, 5’-monophosphate (cAMP) (34). However, mtC5aR1 did not activate ERK1/2 phosphorylation in isolated mitochondria but, rather, diminished ERK1/2 protein concentrations without an effect on the voltage-dependent anion channel 1 (VDAC1), a central entry and exit portal for nutrients in mitochondria (Fig. 3E, and fig. S3G). Constitutive activity of mitochondrial-associated ERK1/2 is a requirement for mitochondrial ATP generation. In line with this, mtC5aR1 stimulation was accompanied by a significant shift away from ATP towards ADP generation (Fig. 3F) and concomitant reduction in cAMP (which is generated form ATP) (Fig. 3G), indicating an overall inhibitory effect of mtC5aR1 on the mitochondrial electron transport chain (ETC) and OXPHOS. Surprisingly, diminished ATP did not trigger phosphorylation of mitochondrial 5’ AMP-activated protein kinase (AMPK), which is typically observed when ATP concentrations drop (35) (Fig. 3E, and fig. S3G).

When faced with limited ATP provision from respiration, cells can generate ATP through glycolysis to meet the bioenergetic demands of effector responses. In fact, high glycolytic activity is a feature of pro-inflammatory monocytes and macrophages (36). We thus hypothesized that mtC5aR1 activation may result in metabolic shift and assessed glycolysis and OXPHOS in human resting and LPS+CC-activated monocytes in the presence or absence of JPE1375. LPS+CC activation significantly augmented glycolysis vs. coupled (ATP-producing) respiration (Fig. 3H). This was dependent on mtC5aR1 as the effect was lost upon intracellular C5aR1 inhibition (Fig. 3H). Interestingly, although intracellular C5aR1-mediated signals are required for nigericin-driven IL-1β production, nigericin induced distinct metabolic profiles, which seem rather potentiated by mtC5aR1 inhibition,

compared to those driven by sensing crystals, (fig. S3H). Thus, metabolic adaptations initiated by intracellular mtC5aR1 seem adjusted according to the nature of the sensed DAMP.

The observed reduction in glycolysis upon intracellular C5aR1 inhibition was not due to limitation of glucose flux as neither expression of the glucose transporter GLUT1 (fig. S3I and J) nor the uptake of glucose was reduced (Fig. 3I and fig. S3K). As expected, inhibition of glycolysis by 2-DG strongly reduced IL-1β production by human LPS+CC-activated monocytes with or without JPE1375 addition to cultures (37) (fig. S3K and L). Hexokinases (HK) I and II are initial enzymes of glycolysis and catalyze generation of glucose-6-phoshate (G6P) from glucose. HKs can be mitochondria-associated where they control VDAC channel opening, mitochondrial integrity, cell survival and NLRP3 activation (38, 39). Silencing of *C5AR1* in human macrophages reduced the release of HKI from mitochondria in resting and in LPS+CC-activated cells, presumably due to reduced glycolysis (39) (fig. S3M and N). Together, these data indicate that inhibition of intracellular C5aR1 does not impair glucose uptake and initiation of glycolytic flux but rather directly impacts mitochondrial activity. Consistent with this, while the expression of C5aR1 on mitochondria did not change during priming or crystal-sensing (fig. S3O), inhibition of mtC5aR1 function by JPE1375 affected mitochondrial mass and dynamics (Fig. 3J to N). Importantly, while high LPS doses normally induce mitochondrial mass (as a measure of biogenesis) in macrophages (40) and fig. S3P), the priming and CC-sensing conditions used here to evoke IL-1β production rather led to a decrease in mitochondrial mass (Fig. 3J and fig. S3Q). Pre-incubation of cells with JPE1375 had no effect on mitochondrial mass in activated cells but JPE1375 surprisingly increased mitochondrial biogenesis in resting cells (Fig. 3J and fig. S3Q). Assessment of mitochondrial morphology (41) in CC-sensing THP-1 cells by confocal microscopy (Fig. 3K) supported a role for the mtC5aR1 in directing mitochondrial dynamics. We confirmed that mtC5aR1 inhibition increased the mitochondrial footprint (mass) in resting cells (Fig. 3L) and found that mtC5aR1 blockage decreased mitochondria intensity in activated monocytes (in line with mitochondrial mass increase normally accompanying IL-1β generation (42)) (Fig. 3M). Moreover, upon CC-sensing, mitochondria repositioned within cells to assume a perinuclear localization and JPE1375 treatment led to an increase in the mitochondrial network size (Fig. 3N) without affecting branch length or size (fig. S3R). In sum, these data show that C5aR1 engagement on mitochondria changes their dynamics and tips the balance of cellular ATP generation from the ETC to glycolysis, which typically favors pro-inflammatory IL-1β production, during crystal sensing.

High fat diet-induced atherosclerosis is driven by macrophage-expressed C5aR1

We next thought to address the significance of macrophage IL-1β induced during sterile inflammation by C5aR1. A hallmark of ACVD is accumulation of CC-loaded, pro-inflammatory macrophages in lesional plaques. Success in reducing ACVD in mouse models using NLRP3 or IL-1β inhibitors demonstrate a key pathogenic role for IL-1β (43). Bone marrow-derived macrophages (BMDMs) from global *C5ar1*$^{-/-}$ mice showed reduced mature IL-1β secretion upon *in vitro* CC-sensing when compared to wild type macrophages (Fig. 4A, and fig. S4A). We next exposed 10–12-week-old male and female atherosclerosis-

prone mice (global *Ldlr*$^{-/-}$) that had a specific deletion of *C5ar1* in myeloid cells only (*Ldlr*$^{-/-}$*C5ar1*$^{fl/fl}$*LyzM-Cre*$^{+/-}$, referred to as *Ldlr–mC5ar1*$^{-/-}$) and *Ldlr*–control mice (*Ldlr*$^{-/-}$*C5ar1*$^{fl/fl}$*LyzM-Cre*$^{-/-}$) to a high fat (cholesterol) Western diet (high fat diet, HFD) for 12 weeks. Animals were then euthanized and their hearts (aortic roots) and whole aortas harvested (Fig. 4B). We observed ~50% less atherosclerosis in the entire aortic area in *Ldlr–mC5ar1*$^{-/-}$ mice compared to the *Ldlr*$^{-/-}$–control animals (Fig. 4C and D). This effect was sex-specific, as only male mice displayed a significant reduction in lesions, while female mice were not protected (Fig. 4E). This was neither due to differences in circulating very low-density lipoprotein (VLDL), low-density lipoprotein (LDL) or high-density lipoprotein (HDL) at the beginning of the HFD (Fig. 4F), nor to differences in total cholesterol or triglyceride levels between male and female mice (fig. S4B). Also, primed BMDMs derived from male and female *Ldlr–mC5ar1*$^{-/-}$ animals produced comparable amounts of mature IL-1β upon CC exposure (fig. S4C). In line with protection against plaque formation, male *Ldlr-mC5ar1*$^{-/-}$ mice failed to display the increase in total cholesterol levels normally seen upon HFD and ACVD and that we observed as expected in control mice (Fig. 4G). Female *Ldlr–mC5ar1*$^{-/-}$ mice, which were not protected from ACVD, showed incremented serum cholesterol levels, similar to control mice (fig. S4D).

Focusing on the male mice, we also observed fewer necrotic areas in the cross sections of the aortic roots of *Ldlr–mC5ar1*$^{-/-}$ mice compared to control mice (Fig. 4H and I). Further, *C5ar1* mRNA levels in the whole aortas of male and female *Ldlr*$^{-/-}$ mice that had been fed a HFD were increased compared to animals on standard chow, while *C5ar2* mRNA levels encoding the alternative C5a receptor 2 (C5aR2, classically regarded as a C5aR1-inhibitory receptor (19)), were decreased (fig. S4E). This shift in balance of C5aR1 versus C5aR2 expression was also observed in splenic Ly6C^{hi} monocytes which are hallmark cells of atherosclerosis induced by hypercholesterolemia (fig. S4F). Inflammation-induced macrophages analyzed *ex vivo* retained predominantly intracellular expression of the C5aRs (fig. S4G), suggesting that intracellular C5aR1 engagement in myeloid cells during sterile inflammation can readily occur *in vivo*. In summary, we found myeloid cell-specific *C5ar1* activity to be a driver of ACVD induced by a Western diet.

Cell-autonomous C5 drives metabolic adaption and IL-1β secretion upon crystal-sensing

We next explored if IL-1β produced by monocytes or macrophages in mice also requires mitochondrial C5aR1 signaling, similar to our observations in human myeloid cells. We confirmed mitochondrial expression of C5aR1 in mouse BMDMs (fig. S5A). We utilized cells from mouse strains that expressed the LDL receptor normally but lacked C5aR1 (44) specifically in myeloid cells (*C5ar1*$^{fl/fl}$*LyzM-Cre*$^{+/-}$*, mC5ar1*$^{-/-}$) and a matching control strain. We included in this analysis BMDMs from a new, custom-generated, floxed YFP-C5 Reporter mouse, crossbred to LyzM-cre mice (*C5*$^{fl/fl}$*LyzM-cre*$^{+/-}$*, mC5*$^{-/-}$) (fig. S5B to D) and a matching control strain to assess the role of cell-intrinsic C5 in crystal-induced IL-1β production by mouse macrophages. In line with our data derived from human monocytes and non-differentiated macrophages, primed BMDMs from male and female *mC5ar1*$^{-/-}$ and *mC5*$^{-/-}$ animals produced significantly less IL-1β (Fig. 5A) and mitochondrial ROS (Fig. 5B) upon CC exposure when compared to their respective control strain cells. Addition of recombinant mouse C5a to activated cultures did not rescue reduced IL-1β production (Fig.

5C). Cell viability was unaffected by C5aR1 or C5 deficiency (fig. S5E), although we noted an increase in cell death in primed BMDMs from all four mouse strains upon CC uptake. Mitochondrial integrity seemed unaltered in C5aR1 or C5-deficient BMDMs because the release of cytochrome c was comparable among cells from all animal strains, with exception of C5-deficient cells, that had augmented cytochrome c release upon LPS+CC stimulation (fig. S5F). Seahorse analysis of C5aR1- or C5-deficient BMDMs showed that both responded with defective glycolysis during LPS priming and upon CC-sensing (Fig. 5D and E). Of note, primed C5- but not C5aR1-deficient BMDMs also displayed a significant reduction in OXPHOS after CC exposure as well as reduced mitochondrial ROS production in the steady state (Fig. 5E), suggesting that macrophages lacking C5 have additional metabolic perturbations when compared to C5aR1-deficient macrophages during activation. Taken together, these data indicate that monocyte- and macrophage-expressed mtC5aR1, engaged by cell-autonomous intracellular C5a generation, is a key contributor to the sterile inflammation underlying atherosclerotic disease driven by a HFD.

Macrophage intracellular C5aR1 activity broadly controls sterile inflammation

To solidify the contributions of the myeloid cell-autonomous C5 system to pro-inflammatory responses during sterile inflammation, we performed two additional sets of *in vivo* experiments in a folic acid (FA)-induced acute kidney injury (AKI) model and thioglycolate-induced peritonitis model. FA-induced AKI is characterized by an inflammatory phase mediated by innate immune cells followed by tissue fibrosis and kidney dysfunction (45). Because complement plays a role in FA-induced AKI, we first utilized male and female $mC5^{-/-}$ mice in this model (Fig. 6A). In line with reduced pro-inflammatory capacity of C5-deficient macrophages upon CC-sensing (Fig. 5A), $mC5^{-/-}$ mice had significantly lower serum creatinine concentration and blood urea nitrogen at the peak of disease (day 2), indicating less severe AKI compared to control animals (Fig. 6B and C). Measurement of collagen and fibronectin expression (as markers of fibrosis) in the kidneys of animals harvested at day 14 post FA injection showed a trend towards their reduced expression (Fig. 6D). The histomorphology of kidneys from $mC5^{-/-}$ mice harvested on day 14 showed mild histomorphologic alterations following FA, while samples from control animals demonstrated fibrosis and concomitant tubular dilatation and an overall higher pathology score (Fig. 6E and F). Therefore, deficiency in myeloid cell C5 was protective during FA-induced AKI. Furthermore, RNA-seq analysis of monocytes isolated from the kidneys of mice after AKI induction showed perturbed OXPHOS gene expression (Fig. 6G and Data file S2), in line with a role for cell-intrinsic C5 in mitochondrial biology.

To compare $mC5ar1^{-/-}$ and $mC5^{-/-}$ mice directly in a sterile inflammation model, we induced peritonitis via thioglycolate injection in both strains and corresponding control animals (fig. S6A). Neutrophil, monocyte and macrophage composition in the exudate was similar among all strains, with the exception that $mC5ar1^{-/-}$ mice had reduced numbers of CD11b-intermediate macrophages (fig. S6B). Unexpectedly though, in this model, LPS-stimulated macrophages from both $mC5ar1^{-/-}$ and $mC5^{-/-}$ mice displayed significantly reduced secretion of TNF but an increase in IL-1β production (fig. S6C and D). We noted no changes in IL-6 (fig. S6C) or in IL-4 and IL-10 (fig. S6C) secretion, suggesting no gross M1 vs. M2 imbalance among the animals lacking C5 or C5aR1 in myeloid cells. Stimulated

C5aR1 and C5-deficient macrophages, however, also had augmented mitochondrial ROS production (fig. S6E), a trend towards increased cytosolic cytochrome c levels (fig. S6F), and reduced viability (fig. S6G), all features that are associated with heightened IL-1β production. Thus, while C5 and C5aR1-deficient macrophages display a congruent *in vivo* phenotype during thioglycolate-induced peritonitis, in this model, the cell-intrinsic C5-C5aR1 axis drives TNF production and restrains IL-1β generation.

Overall, our data indicate that the cell-autonomous C5 system is an important regulator of monocyte and macrophage IL-1β production during sterile inflammation. Depending on the nature and location of the inflammation trigger, however, C5aR1 may exert positive or negative effects on IL-1β production.

Intracellular C5aR1 activity supports the inflammatory milieu of atherosclerotic plaques

Last, we probed whether our findings surrounding this intracellular C5aR1 (maladaptive) activity may extend to human disease. For this, we focused on the IL-1β-driving role of the mtC5aR1 in ACVD. We first obtained atherosclerotic carotid plaques through carotid endarterectomy of male and female patients with defined ACVD (table S1). Such freshly isolated plaques contain immune cells of which inflammatory macrophages and activated T cells represent the dominant immune cell populations and display evidence of active IL-1β signaling (46). Dissolving CC in isolated plaques by addition of β-cyclodextrin has been shown to trigger the normalization of expression of genes encoding for inflammatory mediators including key complement components and *IL1B* and *NLRP3* (47). We hence *ex vivo* cultured isolated plaques in the presence of either extracellular (PMX53) or extra- and intracellular (JPE1375) C5aR1 inhibitors or carrier overnight and measured cytokines secreted into the supernatant by plaque-resident cells. We also performed RNA-sequencing analyses of the differently treated plaques (Fig. 7A). In line with our *in vitro* data (Fig. 1), treatment of plaques with the cell-permeable C5aR1 inhibitor JPE1375 but not with the non-cell-permeable inhibitor PMX53 significantly reduced IL-1β generation (Fig. 7B). Other cytokines known to contribute to the specialized environment of carotid plaques, such as TNF, granulocyte-colony stimulating factor (G-CSF), IL-6, IL-5 and anti-inflammatory IL-1Ra remained unaffected by either treatment (Fig. 7B, and fig. S7). Neither C5aR1 inhibitor treatment affected the viability of cells in the plaques (Fig. 7C), and we confirmed that monocytes or macrophages represented the majority of immune cells within the plaques (Fig. 7D). Interestingly, treatment with either the cell-permeable or non-cell permeable C5aR1 inhibitor reduced the production of fibroblast growth factor (FGF), a hallmark growth factor of macrophages in advanced atherosclerotic lesions (48, 49). This observation may indicate that surface C5aR1 activity of macrophages in plaques serves a specific function connected to FGF biology (fig. S7). Anti-inflammatory IL-10 secretion was also reduced by JPE1375 treatment (Fig. 7B), in line with the presence of M1 macrophages in developing plaques (50) and our finding that JPE1375 reduced M1-generated IL-10 (fig. S1S).

To further explore the JPE1375-driven mechanism(s), we performed RNA-sequencing of the plaques treated with carrier or JPE1375. JPE1375 treatment had, as expected, a predominantly inhibitory effect on gene expression in plaque-resident cells, down-regulating

453 genes (Fig. 7E, and Data file S1). Congruent with our *in vitro* data, the inhibition of genes encoding for the general inflammatory response, including that of complement and TNF signaling were among the most enriched hallmark pathways in carrier-treated cells versus JPE1375-exposed cells (Fig. 7F and G). Further aligning with a role for the mtC5aR1, we also noted significant changes in the genes encoding proteins that participate in mitochondrial membrane activity (Fig. 7H). Additionally, cholesterol metabolism and lipid pathways underlying atherosclerosis were among the top Kegg pathways normalized by JPE1375 treatment (Fig. 7I). Assessment of the immune cell type connected with the observed gene changes indicated that myeloid cells and monocytes and macrophages were indeed the predominant populations responding to JPE1375 treatment (Fig. 7J). *C5AR1* gene expression itself was reduced by the C5aR1 inhibitor, indicative of the existence of a positive C5 system feed-back loop during chronic inflammation in immune cells (Fig. 7K).

To better understand the *in vivo* role played by these pathways in plaque-resident cells, we sourced independent public RNA-sequencing samples from “stable” and “unstable” regions dissected from carotid plaques obtained during carotid endarterectomy in symptomatic patients (51). Macroscopic visible zones of plaque rupture had been categorized as unstable regions. Unstable plaques displayed an engaged inflammatory C5aR1 activation signature: *C5AR1* expression was significantly higher in unstable plaques compared to stable plaques (Fig. 7L) and inflammatory responses, which included complement and TNF signaling were among the most enriched (top ten) hallmark pathways in unstable versus stable plaques (Fig. 7M and N). Moreover, the cellular response signature of unstable plaques was also characterized by predominantly myeloid cells and monocytes and macrophages (Fig. 7O) and increased cholesterol and lipid metabolism (Fig. 7P). Together these data suggest that local/intracellular complement activity and particularly mtC5aR1 signaling in myeloid cells (Fig. 8) is a major contributor to high fat diet-induced ACVD in humans.

DISCUSSION

Sustained complement activation, triggered by endogenous DAMPs or by non-infective irritants has long been identified as a driver of sterile inflammation underlying, for example, gout, kidney fibrosis, and atherosclerosis (16, 23, 52–55). C5aR1 is particularly relevant to sterile inflammation because activation of C5aR1 on endothelial cells during heightened complement activation induces an inflammatory state in these cells, while C5aR1 activation on innate immune cells fosters attachment to the inflamed endothelium, uptake of antigen, tissue infiltration and induction of a pro-inflammatory effector phenotype (56). These events together sustain chronic pathologic tissue inflammation. Inflammation-driving C5aR1-mediated signals on myeloid cells are currently thought to solely originate from cell surface-expressed C5aR1. Here, we show that the C5aR1 is also present on mitochondria in monocytes and macrophages and that intracellular mtC5aR1 stimulation critically contributes to myeloid IL-1β responses underlying sterile inflammation. These data align well with previous observations that cyclodextrin promotes regression of atherosclerosis, at least in part, via reducing intrinsic complement activity in plaque-resident macrophages (47). The unexpected role of intracellular C5 in driving mtC5aR1 signaling in myeloid cells may explain why reducing C5 activation in the plasma of patients with ACVD has not proven clinically beneficial (57). Furthermore, a better understanding of the

functions of complement in sterile chronic inflammation and specifically its role in IL-1β biology may help in developing alternate therapeutic strategies. For example, although the CANTOS study demonstrated that inhibiting IL-1β (a well-established driver of ACVD) therapeutically reduced CVD events in patients with atherosclerosis, the effects were more modest than anticipated and accompanied by a high incidence of fatal infections (43).

Our studies demonstrated not only the broad importance of intracellular C5aR1 for DAMP sensing in several disease models, but also showed that mtC5aR1 signaling has non-uniform effects on cytokine production by monocytes and macrophages. For example, during thioglycolate-induced peritonitis, the macrophage cell-intrinsic C5 system restrained ROS and IL-1β production (fig. S6) and enhanced TNF generation. Thus, the net outcome of mtC5aR1 stimulation on IL-1β production during sterile inflammation appears to be dependent on the integration of upstream, lateral, and downstream signals. These involve the sensing monocyte or macrophage sub-population, the nature and strength of the DAMP trigger (likely dictating the cellular C5a concentrations) and cross-engagement with other PRR sensor systems (58). In fact, earlier studies utilizing global *C5ar1*$^{-/-}$ mice and different pathogen dosages also noted that C5aR1 deficiency reduced mouse BMDM but increased peritoneal monocyte IL-1β production upon TLR4 activation in models of sepsis (59, 60). The differences in the outcome of myeloid cell responses to mtC5aR1 engagement is likely due to distinct C5aR1 (or other complosome component) expression signatures among monocytes, macrophages and dendritic cells, as have been noted in both mice and humans (61–64), and/or to distinct metabolic sensors engaged (65). For example, in human M2, but not M1, macrophages, ATP sensing is uncoupled from the NLRP3 inflammasome and IL-1β production is controlled by ROS and the cytoskeleton (66). Accordingly, we also found IL-1β suppression only in M2, but not M1, macrophages upon mtC5aR1 blockade. Conversely, mtC5aR1 inhibition reduced IL-10 production in differentiated M1, but not M2, macrophages (fig. S1). The latter finding probably explains the impact of C5aR1 inhibition on both IL-1β and IL-10 (and possibly also on the TNF pathway gene signature) of plaque-resident myeloid cells from the CVD patients, as the plaques harbor a mixture of M1 and M2 (and other) macrophage populations (67).

The identification of the C5aR1 as a mitochondrial modulator of ROS production and glycogenic vs. non-glycogenic ATP generation aligns with the emerging role of the complosome as orchestrator of basic biochemical and particularly metabolic reactions. Such non-canonical intracellular functions of complement are consistent with the fact that other ancient PRR systems are also involved in basic physiological processes of the cell (68, 69). Conceptually, our findings are also in line with the fact that a large proportion of GPCRs (or receptors in general) operate at the cell surface and within intracellular compartments and that the location of their engagement may dictate the nature of signaling pathways induced (30). Of note, C5aR1 does not contain a canonical mitochondrial targeting signal and the molecular mechanism directing C5aR1 subcellular trafficking is unknown, but may be an interesting area of future research.

Of importance will also be to further define the diverse triggers and modes of mtC5aR1 engagement *in vivo* during sterile inflammation (for example, the response to apoptotic cell sensing) in more depth for potential therapeutic intervention. Here, we explored a model in

which monocytes ingest CC and engage the C5-NLRP3 inflammasome axis rather rapidly to trigger IL-1β production. However, mtC5aR1 activity may also be engaged in a more gradual fashion: Western diet induces the accumulation of minimally modified (mmLDL) or oxidized (oxLDL) LDL in macrophage lysosomes over time, where they eventually form crystal (70). Thus, sustained LDL uptake may continuously enhance C3/C5 convertase formation, intracellular C5a generation and mtC5aR1 activation resulting in a chronic pro-inflammatory and high IL-1β-producing macrophage phenotype. This model also aligns with our observation that C5a is, at least in parts, localized to lysosomes. Mitochondria and lysosomes engage in a heavy crosstalk via the dynamic formation of inter-organelle membrane contact sites. Perturbations in this interaction underlies multiple human diseases (71). Such contact sides would also provide a basis for a controlled C5a and mtC5aR1 interaction that may increase during CC accumulation. Another possibility supporting the C5a-mtC5aR1 interaction could be rupture of CC-loaded lysosomes in over-loaded, stressed, monocytes (72), which could release C5a to engage C5aR1 expressed by mitochondria in the vicinity. The latter scenario could potentially employ other complosome components, such as intracellular C1q (73–75) and/or activated C2 and C4 proteins in an autocrine fashion (fig. S2) and further underpins the need to define complosome activities across cells.

In addition, although we have focused here mostly on mtC5aR1 regulating ROS and ATP production, we have likely only explored one facet of mtC5aR1 activity. Mitochondrial-associated HKs control several key cell physiological events such as cell death, entry of anionic metabolites into mitochondria, mitophagy, antioxidant defense and mitochondrial dynamics (38, 39, 76–78). MtC5aR1-controlled release of mitochondrial-associated HKI observed here (Fig. 3K) could indicate that mtC5aR1 may also impact on other important cellular processes. Indeed, we noted that mtC5aR1 restrains mitochondrial biogenesis in resting monocytes. This suggests that mtC5aR1 may also play a homeostatic role in these cells, a function that we previously established for the intracellular C3aR in T cells (1).

Overall, we suggest that these data have implications beyond understanding the molecular mechanisms underlying sterile inflammation, as mitochondrial function is a central node for cellular stress sensing and control of viability in a broad range of acute and chronic inflammatory responses. Further, it is probable that intracellular C5aR1/mtC5aR1 signaling is also engaged during sensing of PAMPs such as intracellular pathogens (as has recently be shown for intracellular C3 (25, 79)) and is, therefore, also involved in infection control. Thus, therapeutic targeting of intracellular C5aR1 and/or the intracellular C5 system may have the potential to restore mitochondrial function and reduce inflammation-mediated tissue injury in multiple disease settings.

MATERIALS AND METHODS

Study design

This study aimed to investigate if human monocytes harbor and engage components of an intracellular, cell intrinsic, C5 system to produce IL-1β during sensing of endogenous danger and induction of sterile inflammation. We selected the sensing of crystals in form of cholesterol (or monosodium urate (MSU)) crystals and measured the impact of inhibition of C5 expression, intracellular C5a generation, or intracellular C5aR1 engagement via siRNA

technique or application of specific inhibitors on IL-1β production by purified human monocytes and macrophages *in vitro*. *In vivo* significance of observations derived from these experiments were confirmed by: 1. Using mice with deletions of the *C5ar1* or the *C5* gene in myeloid cells only, in *in vivo* models of sterile inflammation, including a high fat diet-induced atherosclerosis model, a folic acid-induced kidney injury model, and a thioglycolate-induced peritonitis model, and 2. By assessing the impact of intracellular C5aR1 inhibition on inflammatory cytokine production and RNAseq of cells residing in the carotid plaques of patients with atherosclerosis (n=5) *ex vivo*.

Healthy donors and patients

Whole blood samples were obtained and processed with ethical and institutional approvals. For healthy donors, freshly drawn blood or buffy coats were obtained from the NIH Blood Bank, Bethesda, USA and from St. Olavs Hospital, Trondheim, Norway, the Health Authorities of South-Eastern Norway (REC number S-04114). All healthy donors gave informed consent prior to sample collection (male and female donors between 27 and 65 years of age). Five patients with advanced atherosclerosis (see Table S1) were recruited at Rikshospitallet, Oslo, Norway (study approval REC number 2014/2078). As part of the ultrasound examination, the total extracranial part of the carotid artery was examined with B-mode and Doppler analyses. Ultrasound plaque appearance in terms of echogenicity was classified according to consensus criteria (80). Mean age of the study population was about 67 years, and three patients were male and two females. Exclusion criteria were heart failure, liver disease, kidney disease, and severe concomitant disease such as infection, connective tissue disease, or malignancy.

Mice

The *C5ar1*$^{Fl/Fl}$ *LyzM*^{cre} mice were provided via Michail S. Lionakis (NIAID, NIH) by Jörg Köhl (University of Lübeck, Germany). The *C57BL/10 Ldlr*$^{-/-}$ mice were obtained from Taconic. We generated *Ldlr*$^{-/-}$ mice lacking C5aR1 expression specifically in myeloid cells, including monocytes and macrophages, by crossing *Ldlr*$^{-/-}$ mice with *C5ar1*$^{-/-}$ *Lyz-M*^{cre} animals. The new floxed *C5*-Yellow Fluorescent Protein (*C5*-YFP) reporter mouse strain was custom-generated by genOway (Lyon, France) and the methodological approach is summarized in Supplementary Figure 5. These mice were bred to *Lyz-M*^{cre} animals to generate mice lacking C5 expression only in myeloid cells. All animals were maintained in AALAC-accredited BSL2 or BSL3 facilities at the NIH and experiments conducted in accordance with the GSK Policy on the Care, Welfare and Treatment of Laboratory Animals and were reviewed by the Institutional Animal Care and Use Committee either at GSK or by the ethical review process at NIH and performed in compliance with an animal study proposal approved by the NHLBI Animal Care and Use Committee.

Human monocytes, macrophages, and THP-1 cell line

Monocytes were isolated from blood using the MACS Human CD14^{+} Positive Isolation Kit (Miltenyi, Biotech Ltd, Bisley, UK). CD14^{+} cells were consistently > 98% pure and were cultured in 24-well culture plates (5.0×10^5 cells/well) in media containing 10% heat-inactivated serum. Monocytes were primed with LPS (500 pg/ml) for 2 hrs and stimulated with CC (500 μg/ml), MSU (150 μg/ml), Nigericin (5 μg/ml) or PBS for 4–6 hrs. To obtain

human monocyte-derived macrophages (hMDM), $CD14^+$ cells were cultured in medium supplemented with M-CSF (20 ng/ml) for six days with medium change after three days. *Human M1 and M2 macrophages* were generated from purified monocytes (see above). Monocytes were plates at 0.5×10^6 cells in a 24-well plate and supplemented with 20 ng/mL of human GM-CSF (PeproTech, Rocky Hill, NJ; 300–03) for M1 differentiation, or with 20 ng/mL of human M-CSF (PeproTech, 300–25) for M2 differentiation. Media, including respective M1 or M2-driving growth factors, was refreshed on day 3. At day 6, M1 macrophages were further polarized with 100 ng/mL human IFN-γ (PeproTech, 300–02) and 50 ng/mL LPS and M2 macrophages with 20 ng/mL IL-13 (PeproTech, 200–13) and 20 ng/mL IL-4 (PeproTech, 200–04) for 24 hrs. Stimulation with LPS and/or CC (500 μg/ml) was performed for 4 hrs the next day and cytokines produced by M1 or M2 measured using the LEGENDplex Human Macrophage/Microglia (13-plex) with Filter Plate (Biolegend, San Diego, CA; Cat# 740502), according to the manufacturer's protocol. *THP-1* (ATCC, TIB-202) differentiated into a macrophage-like phenotype with PMA (Sigma Aldrich, P1585; 50 ng/ml) were primed with LPS (100 ng/ml) for 2 hrs and stimulated with CC (500 μg/ml), MSU (150 μg/ml) or nigericin (5 μg/ml) for 8 hrs. Where C5aR1 agonists and/or antagonists and/or the cell-permeable Factor B inhibitor were used, cells were pretreated for 1 hr with the selected compound(s) prior to priming with LPS and further stimulation with CC, MSU or nigericin. Cell supernatants and cell pellets were harvested for multiplex cytokine or Western blot analysis and stored at −80 °C.

Human carotid plaques

Atherosclerotic carotid plaques were collected during carotid endarterectomy. Biopsies from atherosclerotic carotid plaques were placed in Dulbecco's modified Eagle's medium (D-MEM/F12; Gibco) enriched with 30 mg/ml endotoxin-free and fatty acid-free bovine serum albumin (Sigma Aldrich). The biopsies containing atherosclerotic plaques of each patient were split into macroscopically equal pieces and treated with non-cell permeable C5aR1 antagonist PMX53 (10 μM), cell permeable C5aR1 antagonist JEP1375 (1μM) or PBS for 6 hrs. Supernatants were harvested for multiplex cytokine analysis and snap frozen plaques were stored at −80 °C.

Mouse macrophages

To generate bone marrow-derived macrophages (BMDMs), single cell suspensions of bone marrow cells from WT, global *C5ar1*$^{-/-}$ mice, *Ldlr*- and myeloid *C5ar1*-deficient mice (*Ldlr*$^{-/-}$ *C5ar1*$^{Fl/Fl}$ *LyzM-cre*$^{+/-}$*; Ldlr–mC5ar1*$^{-/-}$) and control mice (*Ldlr*$^{-/-}$ *C5ar1*$^{Fl/Fl}$ *LyzM-cre*$^{-/-}$), and myeloid *C5*-deficient mice (*C5*$^{Fl/Fl}$ *LyzM-cre*$^{+/-}$*; mC5*$^{-/-}$) and control mice (*C5*$^{Fl/Fl}$ *LyzM-cre*$^{-/-}$) were generated and red blood cells lysed using ACK lysis buffer (Life Technologies). Cells were plated in 96-well culture plates in media containing 10% heat-inactivated serum supplemented with mouse M-CSF (20 ng/ml) for 6 days with a medium change after day three. BMDM were primed with LPS (100 ng/ml) for 2 hrs and stimulated with CC (500 μg/ml) or MSU (150 μg/ml) for 6 hrs. Supernatant was harvested and stored at −80 °C until further analysis. Thioglycolate-elicited peritoneal macrophages were isolated via aspiration of cells from the peritoneal cavity of euthanized mice 3 days after thioglycollate i.p. injection and enriched by panning in 48-well culture plates for 2 hrs at 37 °C.

Mouse high fat diet

Unless indicated otherwise, all mice received a standard non-atherogenic rodent chow. For dietary intervention studies, experimental mice were fed a Western type (high fat) diet containing 21% milk fat and 0.2% cholesterol (E15721–347, Ssniff Spezialdiäten GmbH, Soest, Germany) for 10–12 weeks.

Thioglycollate-induced peritonitis

For the induction of sterile peritonitis, mice were intraperitoneally injected with a single dose of

2% sterile thioglycolate solution (in 0.3M NaHCO3, volume of 200uL; stock solution was allowed to age for three weeks at room temperature in the dark before injection) and sacrificed 72 hrs post injection for isolation and characterization of thioglycolate-elicited peritoneal macrophages.

Cytokine and chemokine measurements

Secreted human IL-1β and IL-10 were measured using the Human IL-1β/IL-1F2 DuoSet Kit or the Human IL-10 Quantikine Elisa kit (R&D Systems, DY201 and D1000B, respectively). Additional cytokines, growth factors and proteins (TNF, G-CSF, IL-6, IL-5, FGF, Arginase, IL-1RA, etc.) were quantified using a custom-assembled Human Multiplex Cytokine Assay (Bio-Plex; Bio-Rad Laboratories Inc.). Mouse IL-1β measured by either utilizing the Mouse IL-1 beta/IL-1F2 DuoSet ELISA kit (R&D Systems, DY401; recognizes predominantly mature IL-1β), via intracellular staining, or with the LEGENDplex™ Mouse Inflammation Panel (13-plex) (BioLegend, 140150). The latter kit was also used to assess the additional mouse cytokines measured in this study.

Activation of purified mitochondria

The crude mitochondrial (Mc) fraction was further assessed for responsiveness towards C5a activation. Purified Mc were resuspended in mitochondria resuspension buffer prepared according to Wieckowski *et al.*(81). The solution containing Mc was distributed into equal volumes and treated with buffer or with increasing amounts of serum purified C5a (5–100 ng/ml, CompTech) at 30 °C with and without inhibitors for indicated time points. Mitochondria were then pelleted at 7000 × *g*, washed, and utilized in subsequent desired assays.

Confocal microscopy of isolated mitochondria

Mitochondrial fractions were fixed and permeabilized using the Fixation/Permeabilization kit (BD Biosciences) and stained with the indicated primary antibodies: anti-C5aR1 (1 μg/ml) and anti-TOM20 (1 μg/ml) overnight. After blocking with 20 % human serum, Mc were stained for 1 hr, at 4 °C, with highly cross-absorbed secondary antibodies (Invitrogen), at a concentration of 1 μg/mL: goat anti-mouse IgG (H+L) Alexa Fluor 488 (A11034) and goat anti-rabbit Atto 647N (Sigma Aldrich). Mc were mounted on coverslips using ProLong Diamond antifade mountant (Invitrogen, P36970), and images acquired using a Leica SP8 STED 3x microscope (Leica Microsystems) with usage of Huyguens and ImageJ softwares

for image processing. Images were acquired as Z-stacks, through a 63x/1.4 oil-immersion objective, using 488 nm, 633 nm white laser lines for detection. Z-stacks images were deconvolved using SVI Huygens before generating single micrographs, with Fiji (version 2.1.0/1.52t) and JaCoP plugin used for detecting C5aR1 and TOM20 colocalization.

Cell death assays

During FACS-based measurements, viability of cells was routinely monitored by cell staining with an appropriate LIVE/DEAD Fixable Near-IR stain (Thermofisher Scientific). *Lactate dehydrogenase (LDH) assay*. Monocytes or macrophages were cultured as indicated in the experiments. Cell death/cytotoxicity, as determined by LDH release, was assayed in culture supernatants using a calorimetric LDH Assay Kit (CyQUANT™ LDH Cytotoxicity Assay; Invitrogen, C20301). *ATP production*. Cell death was also measured using the CellTiter-Glo® 3D Cell Viability Assay (Promega, G9681), which assesses overall ATP production by cells as a measure of viability.

Cytochrome c release measurements

To assess cytoplasmic cytochrome c in human and mouse monocytes or macrophages, the Human Cytochrome c Quantikine ELISA kit (DCTC0) or the Rat/Mouse Cytochrome c Quantikine ELISA kit (MCTC0, both from R&D Systems), respectively, were used according to the manufacturer's protocol.

Glucose uptake measurement

Glucose uptake capacity by resting and crystal-sensing human monocytes was measured by uptake of the fluorescent 2-deoxy-D-glucose analog 2-[N-(7-nitrobenz-2-oxa-1,3-diazol-4-yl)amino]-2-deoxy-D-glucose (2-NBDG; Sigma Aldrich, 72987). Briefly, human monocytes were resuspended in 250 μl RPMI/10 % FCS containing 20 μM 2-NBDG. Cells were either left non-activated, primed with LPS for 2 hrs and then exposed to cholesterol crystals for an additional 2 hrs at 37 °C and 5 % CO_2 prior to washing twice with FACS buffer. 2-NBDG uptake was then assessed by flowcytometry on a FACSCanto II™ (BD Biosciences) and data analyzed using FlowJo (FlowJo, LLC).

ADP, ATP, and cyclic AMP production by mitochondria

Time-course measurement of cyclic adenosine monophosphate (cAMP) generation was performed on purified mitochondria treated with purified C5a (10 or 20 ng/ml) for indicated time points. The Direct cAMP ELISA Kit (Enzo Life Science, ADI-900–066) was used for measurements according to the manufacturer's instructions. For assessment of the ADP/ATP ratio of mitochondria, the ADP/ATP Quantification Bioluminescent Kit (Sigma Aldrich, MAK135) was used, according to the manufacturés protocol.

Mitochondrial reactive oxygen species (ROS) quantification

Purified mitochondria. Isolated crude mitochondria were incubated with 1 μM of CM-H_2TMROS or 5 μM of MitoSOX (Thermofisher Scientific) reagent at 30 °C, for 30 minutes, prior to treatment with PMX53 (10 μM) and activation with C5a (see above). The CM-H_2TMROS or MitoSOX fluorescence was then measured using λex/em= 554⁄576 nm. The

fluorescence intensity measured from mitochondria without CM-H_2TMROS or MitoSOX treatment served as basal background signal and was subtracted before analysis. *Whole cells*. Mitochondrial ROS production in human monocytes was measured by incubating resting or activated cells (LPS (500 pg/ml, 2 hrs) and/or CC (500 mg/ml, 4 hrs) (with or without pre-incubation with either PMX53 or JPE1375, 10 μM each for 45 min at 37 °C) for the final 15 min of culture in 5 μM CellROX™ Green Reagent (Thermofisher Scientific, C10444) in media without FCS and phenol red. Cells were harvested, washed twice in 1 × PBS, and mitochondrial ROS production assessed by flowcytometry. ROS production in mouse BMDM or thioglycolate-elicited macrophages was measured in a similar fashion after appropriate stimulation.

Mitochondrial mass assessment

Human purified monocytes were pre-incubated with either PMX53 or JPE1375 (10 μM) or carrier solution and left non-activated or were primed with LPS (500 pg/ml, 2 hrs) and/or CC (500 mg/ml, 4 hrs). The media was then removed and replaced with pre-warmed media without FCS containing 10 nM of MitoTracker™ Green FM and 50 nM of MitoTracker™ Red FM (Thermofisher Scientific) for 30 min. Cells were washed twice with 1 × PBS and mitochondrial mass (MitoTracker Green) and membrane potential (MitoTracker Red) assessed by flowcytometry. Changes in mitochondrial mass were as via (MFI, MitoTracker Green) / (MFI, MitoTracker Red).

Statistical analyses

Analyses were performed with GraphPad Prism. Data are presented as mean ± SEM and analyzed using either Wilcoxon matched-paired signed rank test, or one-way ANOVA or wo-way ANOVA, with Bonferroni's multiple comparison test, as appropriate. P values < 0.05 denote statistical significance. All experiments were carried out in duplicate technical and biological replicate unless otherwise stated. FACS plots depicted are representative of a minimum of three replicates (n=3).

Supplementary Material

Refer to Web version on PubMed Central for supplementary material.

ACKNOWLEDGEMENTS

We thank the healthy volunteers and the patients for their support. We thank L. Ryan and A. Marstad for initial contribution to the plaque analysis and L. Hoang for Immunogold staining.

Funding:

This work was supported by a Wellcome Trust Investigator Award (C.K), a Wellcome Trust Intermediate Clinical Fellowship award (B.A.), the National Institute for Health Research (NIHR) Biomedical Research Centre based at Guy's and St Thomas' NHS Foundation Trust and King's College London, in part by the Division of Intramural Research (C.K.) and extramural Research (5K22HL125593 to M.K.) of the National Heart, Lung, and Blood Institute, by intramural research of the National Institute of Allergy and Infectious Diseases (M.S.L), extramural research of the National Institute of General Medical Sciences (R35GM138283 to M.K.), NIH, and by grants from the Research Council of Norway through its Centres of Excellence funding scheme Grant 223255/F50 (T.E), the Liaison Committee in Central Norway (50052400) (T.E.), and FRIPRO Mobility Grant 251255/F20 (N.N). C.J.B was supported by the SFB grant InThro F54 funded by the Austrian Science Fund (FWF), M.G.K was supported by the fellowship of the doctoral program Cell Communication in Health and Disease 'CCHD' (DK W1205-B09)

funded by the FWF, and T.F. was supported by the German Research Foundation (DFG fellowship FR-3851/2-1). The RNA library prep and sequencing were performed in close collaboration with the Genomics Core Facility (GCF), Norwegian University of Science and Technology (NTNU). GCF is funded by the Faculty of Medicine and Health Sciences at NTNU and Central Norway Regional Health Authority. The light and electron microscopy data was provided by the Cellular and Molecular Imaging Core Facility (CMIC), Norwegian University of Science and Technology (NTNU). CMIC is funded by the Faculty of Medicine at NTNU and Central Norway Regional Health Authority.

Data and materials availability:

Data related to the gene arrays performed using the carotid plaques from patients with atherosclerosis are deposited with GEO under accession number GSE162389. Data related to the gene arrays performed using monocytes isolated from the kidneys of mice after folic acid-induced KI are deposited with GEO under accession number GSE186545. The cell-permeable factor B inhibitor are available from GlaxoSmithKline under a cooperative research and development agreement (CRADA) with the University/Institution.

All other data needed to evaluate the conclusions in the paper are present in the paper or the Supplementary Materials.

REFERENCES AND NOTES

1. Liszewski MK, Kolev M, Le Friec G, Leung M, Bertram PG, Fara AF, Subias M, Pickering MC, Drouet C, Meri S, Arstila TP, Pekkarinen PT, Ma M, Cope A, Reinheckel T, Rodriguez de Cordoba S, Afzali B, Atkinson JP, Kemper C, Intracellular complement activation sustains T cell homeostasis and mediates effector differentiation. Immunity 39, 1143–1157 (2013). [PubMed: 24315997]
2. Arbore G, West EE, Rahman J, Le Friec G, Niyonzima N, Pirooznia M, Tunc I, Pavlidis P, Powell N, Li Y, Liu P, Servais A, Couzi L, Fremeaux-Bacchi V, Placais L, Ferraro A, Walsh PR, Kavanagh D, Afzali B, Lavender P, Lachmann HJ, Kemper C, Complement receptor CD46 co-stimulates optimal human CD8(+) T cell effector function via fatty acid metabolism. Nat.Commun 9, 4186 (2018). [PubMed: 30305631]
3. Hess C, Kemper C, Complement-Mediated Regulation of Metabolism and Basic Cellular Processes. Immunity 45, 240–254 (2016). [PubMed: 27533012]
4. Kolev M, Dimeloe S, Le Friec G, Navarini A, Arbore G, Povoleri GA, Fischer M, Belle R, Loeliger J, Develioglu L, Bantug GR, Watson J, Couzi L, Afzali B, Lavender P, Hess C, Kemper C, Complement Regulates Nutrient Influx and Metabolic Reprogramming during Th1 Cell Responses. Immunity 42, 1033–1047 (2015). [PubMed: 26084023]
5. West EE, Kolev M, Kemper C, Complement and the Regulation of T Cell Responses. Annu. Rev. Immunol 36, 309–338 (2018). [PubMed: 29677470]
6. Chang CH, Curtis JD, Maggi LB Jr., Faubert B, Villarino AV, O'Sullivan D, Huang SC, van der Windt GJ, Blagih J, Qiu J, Weber JD, Pearce EJ, Jones RG, Pearce EL, Posttranscriptional control of T cell effector function by aerobic glycolysis. Cell 153, 1239–1251 (2013). [PubMed: 23746840]
7. Kolev M, West EE, Kunz N, Chauss D, Moseman EA, Rahman J, Freiwald T, Balmer ML, Lotscher J, Dimeloe S, Rosser EC, Wedderburn LR, Mayer-Barber KD, Bohrer A, Lavender P, Cope A, Wang L, Kaplan MJ, Moutsopoulos NM, McGavern D, Holland SM, Hess C, Kazemian M, Afzali B, Kemper C, Diapedesis-Induced Integrin Signaling via LFA-1 Facilitates Tissue Immunity by Inducing Intrinsic Complement C3 Expression in Immune Cells. Immunity 52, 513–527.e518 (2020). [PubMed: 32187519]
8. Cardone J, Le Friec G, Vantourout P, Roberts A, Fuchs A, Jackson I, Suddason T, Lord G, Atkinson JP, Cope A, Hayday A, Kemper C, Complement regulator CD46 temporally regulates cytokine production by conventional and unconventional T cells. Nat. Immunol 11, 862–871 (2010). [PubMed: 20694009]

9. Ellinghaus U, Cortini A, Pinder CL, Le Friec G, Kemper C, Vyse TJ, Dysregulated CD46 shedding interferes with Th1-contraction in systemic lupus erythematosus. Eur. J. Immunol 47, 1200–1210 (2017). [PubMed: 28444759]
10. Le Friec G, Sheppard D, Whiteman P, Karsten CM, Shamoun SA, Laing A, Bugeon L, Dallman MJ, Melchionna T, Chillakuri C, Smith RA, Drouet C, Couzi L, Fremeaux-Bacchi V, Kohl J, Waddington SN, McDonnell JM, Baker A, Handford PA, Lea SM, Kemper C, The CD46-Jagged1 interaction is critical for human TH1 immunity. Nat. Immunol 13, 1213–1221 (2012). [PubMed: 23086448]
11. Arbore G, West EE, Spolski R, Robertson AA, Klos A, Rheinheimer C, Dutow P, Woodruff TM, Yu ZX, O'Neill LA, Coll RC, Sher A, Leonard WJ, Kohl J, Monk P, Cooper MA, Arno M, Afzali B, Lachmann HJ, Cope AP, Mayer-Barber KD, Kemper C, T helper 1 immunity requires complement-driven NLRP3 inflammasome activity in CD4(+) T cells. Science 352, aad1210 (2016).
12. Zindel J, Kubes P, DAMPs, PAMPs, and LAMPs in Immunity and Sterile Inflammation. Annu. Rev. Pathol 15, 493–518 (2020). [PubMed: 31675482]
13. Duewell P, Kono H, Rayner KJ, Sirois CM, Vladimer G, Bauernfeind FG, Abela GS, Franchi L, Nunez G, Schnurr M, Espevik T, Lien E, Fitzgerald KA, Rock KL, Moore KJ, Wright SD, Hornung V, Latz E, NLRP3 inflammasomes are required for atherogenesis and activated by cholesterol crystals. Nature 464, 1357–1361 (2010). [PubMed: 20428172]
14. Gistera A, Hansson GK, The immunology of atherosclerosis. Nat. Rev. Nephrol 13, 368–380 (2017). [PubMed: 28392564]
15. Chinetti-Gbaguidi G, Colin S, Staels B, Macrophage subsets in atherosclerosis. Nat. Rev. Cardiol 12, 10–17 (2015). [PubMed: 25367649]
16. Pilely K, Rosbjerg A, Genster N, Gal P, Pal G, Halvorsen B, Holm S, Aukrust P, Bakke SS, Sporsheim B, Nervik I, Niyonzima N, Bartels ED, Stahl GL, Mollnes TE, Espevik T, Garred P, Cholesterol Crystals Activate the Lectin Complement Pathway via Ficolin-2 and Mannose-Binding Lectin: Implications for the Progression of Atherosclerosis. J. Immunol 196, 5064–5074 (2016). [PubMed: 27183610]
17. Niyonzima N, Halvorsen B, Sporsheim B, Garred P, Aukrust P, Mollnes TE, Espevik T, Complement activation by cholesterol crystals triggers a subsequent cytokine response. Mol. Immunol 84, 43–50 (2017). [PubMed: 27692470]
18. Elvington M, Liszewski MK, Bertram P, Kulkarni HS, Atkinson JP, A C3(H20) recycling pathway is a component of the intracellular complement system. J. Clin. Invest 127, 970–981 (2017). [PubMed: 28192370]
19. Croker DE, Monk PN, Halai R, Kaeslin G, Schofield Z, Wu MC, Clark RJ, Blaskovich MA, Morikis D, Floudas CA, Cooper MA, Woodruff TM, Discovery of functionally selective C5aR2 ligands: novel modulators of C5a signalling. Immunol. Cell Biol 94, 787–795 (2016). [PubMed: 27108698]
20. Otto M, Hawlisch H, Monk PN, Muller M, Klos A, Karp CL, Kohl J, C5a mutants are potent antagonists of the C5a receptor (CD88) and of C5L2: position 69 is the locus that determines agonism or antagonism. J. Biol. Chem 279, 142–151 (2004). [PubMed: 14570896]
21. Gurung P, Kanneganti TD, Novel roles for caspase-8 in IL-1β and inflammasome regulation. Am. J. Pathol 185, 17–25 (2015). [PubMed: 25451151]
22. Gaidt MM, Ebert TS, Chauhan D, Schmidt T, Schmid-Burgk JL, Rapino F, Robertson AA, Cooper MA, Graf T, Hornung V, Human Monocytes Engage an Alternative Inflammasome Pathway. Immunity 44, 833–846 (2016). [PubMed: 27037191]
23. Samstad EO, Niyonzima N, Nymo S, Aune MH, Ryan L, Bakke SS, Lappegard KT, Brekke OL, Lambris JD, Damas JK, Latz E, Mollnes TE, Espevik T, Cholesterol crystals induce complement-dependent inflammasome activation and cytokine release. J. Immunol 192, 2837–2845 (2014). [PubMed: 24554772]
24. Takahashi M, Ishida Y, Iwaki D, Kanno K, Suzuki T, Endo Y, Homma Y, Fujita T, Essential role of mannose-binding lectin-associated serine protease-1 in activation of the complement factor D. J. Exp. Med 207, 29–37 (2010). [PubMed: 20038603]

25. Yan B, Freiwald T, Chauss D, Wang L, West E, Mirabelli C, Zhang CJ, Nichols EM, Malik N, Gregory R, Bantscheff M, Ghidelli-Disse S, Kolev M, Frum T, Spence JR, Sexton JZ, Alysandratos KD, Kotton DN, Pittaluga S, Bibby J, Niyonzima N, Olson MR, Kordasti S, Portilla D, Wobus CE, Laurence A, Lionakis MS, Kemper C, Afzali B, Kazemian M, SARS-CoV-2 drives JAK1/2-dependent local complement hyperactivation. Sci. Immunol 6, eabg0833 (2021).
26. Mannes M, Dopler A, Zolk O, Lang SJ, Halbgebauer R, Höchsmann B, Skerra A, Braun CK, Huber-Lang M, Schrezenmeier H, Schmidt CQ, Complement inhibition at the level of C3 or C5: mechanistic reasons for ongoing terminal pathway activity. Blood 137, 443–455 (2021). [PubMed: 33507296]
27. Dessauer A, Rother U, Rother K, Freeze-thaw activation of the complement attack phase: II. Comparison of convertase generated C--56 with C--56 generated by freezing and thawing. Acta Pathol. Microbiol. Immunol. Scand. Suppl 284, 83–88 (1984). [PubMed: 6444196]
28. Lubbers R, van Essen MF, van Kooten C, Trouw LA, Production of complement components by cells of the immune system. Clin. Exp. Immunol 188, 183–194 (2017). [PubMed: 28249350]
29. Pandey S, Maharana J, Li XX, Woodruff TM, Shukla AK, Emerging Insights into the Structure and Function of Complement C5a Receptors. Trends Biochem. Sci 45, 693–705 (2020). [PubMed: 32402749]
30. Irannejad R, Tomshine JC, Tomshine JR, Chevalier M, Mahoney JP, Steyaert J, Rasmussen SG, Sunahara RK, El-Samad H, Huang B, von Zastrow M, Conformational biosensors reveal GPCR signalling from endosomes. Nature 495, 534–538 (2013). [PubMed: 23515162]
31. Benard G, Massa F, Puente N, Lourenco J, Bellocchio L, Soria-Gomez E, Matias I, Delamarre A, Metna-Laurent M, Cannich A, Hebert-Chatelain E, Mulle C, Ortega-Gutierrez S, Martin-Fontecha M, Klugmann M, Guggenhuber S, Lutz B, Gertsch J, Chaouloff F, Lopez-Rodriguez ML, Grandes P, Rossignol R, Marsicano G, Mitochondrial CB(1) receptors regulate neuronal energy metabolism. Nat. Neurosci 15, 558–564 (2012). [PubMed: 22388959]
32. Suofu Y, Li W, Jean-Alphonse FG, Jia J, Khattar NK, Li J, Baranov SV, Leronni D, Mihalik AC, He Y, Cecon E, Wehbi VL, Kim J, Heath BE, Baranova OV, Wang X, Gable MJ, Kretz ES, Di Benedetto G, Lezon TR, Ferrando LM, Larkin TM, Sullivan M, Yablonska S, Wang J, Minnigh MB, Guillaumet G, Suzenet F, Richardson RM, Poloyac SM, Stolz DB, Jockers R, Witt-Enderby PA, Carlisle DL, Vilardaga JP, Friedlander RM, Dual role of mitochondria in producing melatonin and driving GPCR signaling to block cytochrome c release. Proc. Natl. Acad. Sci. U S A 114, E7997–e8006 (2017). [PubMed: 28874589]
33. Murphy JE, Padilla BE, Hasdemir B, Cottrell GS, Bunnett NW, Endosomes: a legitimate platform for the signaling train. Proc. Natl. Acad. Sci. U S A 106, 17615–17622 (2009). [PubMed: 19822761]
34. Verschoor A, Karsten CM, Broadley SP, Laumonnier Y, Kohl J, Old dogs-new tricks: immunoregulatory properties of C3 and C5 cleavage fragments. Immunol. Rev 274, 112–126 (2016). [PubMed: 27782330]
35. Acin-Perez R, Salazar E, Kamenetsky M, Buck J, Levin LR, Manfredi G, Cyclic AMP produced inside mitochondria regulates oxidative phosphorylation. Cell. Metab 9, 265–276 (2009). [PubMed: 19254571]
36. Viola A, Munari F, Sanchez-Rodriguez R, Scolaro T, Castegna A, The Metabolic Signature of Macrophage Responses. Front. Immunol 10, 1462 (2019). [PubMed: 31333642]
37. Tannahill GM, Curtis AM, Adamik J, Palsson-McDermott EM, McGettrick AF, Goel G, Frezza C, Bernard NJ, Kelly B, Foley NH, Zheng L, Gardet A, Tong Z, Jany SS, Corr SC, Haneklaus M, Caffrey BE, Pierce K, Walmsley S, Beasley FC, Cummins E, Nizet V, Whyte M, Taylor CT, Lin H, Masters SL, Gottlieb E, Kelly VP, Clish C, Auron PE, Xavier RJ, O'Neill LA, Succinate is an inflammatory signal that induces IL-1β through HIF-1α. Nature 496, 238–242 (2013). [PubMed: 23535595]
38. Wolf AJ, Reyes CN, Liang W, Becker C, Shimada K, Wheeler ML, Cho HC, Popescu NI, Coggeshall KM, Arditi M, Underhill DM, Hexokinase Is an Innate Immune Receptor for the Detection of Bacterial Peptidoglycan. Cell 166, 624–636 (2016). [PubMed: 27374331]
39. Pastorino JG, Hoek JB, Hexokinase II: the integration of energy metabolism and control of apoptosis. Curr. Med. Chem 10, 1535–1551 (2003). [PubMed: 12871125]

40. Kapetanovic R, Afroz SF, Ramnath D, Lawrence GM, Okada T, Curson JE, de Bruin J, Fairlie DP, Schroder K, St John JC, Blumenthal A, Sweet MJ, Lipopolysaccharide promotes Drp1-dependent mitochondrial fission and associated inflammatory responses in macrophages. Immunol. Cell Biol 98, 528–539 (2020). [PubMed: 32686869]
41. Valente AJ, Maddalena LA, Robb EL, Moradi F, Stuart JA, A simple ImageJ macro tool for analyzing mitochondrial network morphology in mammalian cell culture. Acta Histochem 119, 315–326 (2017). [PubMed: 28314612]
42. Mills EL, Kelly B, Logan A, Costa ASH, Varma M, Bryant CE, Tourlomousis P, Däbritz JHM, Gottlieb E, Latorre I, Corr SC, McManus G, Ryan D, Jacobs HT, Szibor M, Xavier RJ, Braun T, Frezza C, Murphy MP, O'Neill LA, Succinate Dehydrogenase Supports Metabolic Repurposing of Mitochondria to Drive Inflammatory Macrophages. Cell 167, 457–470.e413 (2016). [PubMed: 27667687]
43. Ridker PM, Everett BM, Thuren T, MacFadyen JG, Chang WH, Ballantyne C, Fonseca F, Nicolau J, Koenig W, Anker SD, Kastelein JJP, Cornel JH, Pais P, Pella D, Genest J, Cifkova R, Lorenzatti A, Forster T, Kobalava Z, Vida-Simiti L, Flather M, Shimokawa H, Ogawa H, Dellborg M, Rossi PRF, Troquay RPT, Libby P, Glynn RJ, Antiinflammatory Therapy with Canakinumab for Atherosclerotic Disease. N. Engl. J. Med 377, 1119–1131 (2017). [PubMed: 28845751]
44. Wiese AV, Ender F, Quell KM, Antoniou K, Vollbrandt T, König P, Köhl J, Laumonnier Y, The C5a/C5aR1 axis controls the development of experimental allergic asthma independent of LysM-expressing pulmonary immune cells. PLoS One 12, e0184956 (2017). [PubMed: 28931049]
45. Wen Y, Crowley SD, The varying roles of macrophages in kidney injury and repair. Curr. Opin. Nephrol. Hypertens 29, 286–292 (2020). [PubMed: 32235271]
46. Fernandez DM, Rahman AH, Fernandez NF, Chudnovskiy A, Amir ED, Amadori L, Khan NS, Wong CK, Shamailova R, Hill CA, Wang Z, Remark R, Li JR, Pina C, Faries C, Awad AJ, Moss N, Bjorkegren JLM, Kim-Schulze S, Gnjatic S, Ma'ayan A, Mocco J, Faries P, Merad M, Giannarelli C, Single-cell immune landscape of human atherosclerotic plaques. Nat. Med 25, 1576–1588 (2019). [PubMed: 31591603]
47. Zimmer S, Grebe A, Bakke SS, Bode N, Halvorsen B, Ulas T, Skjelland M, De Nardo D, Labzin LI, Kerksiek A, Hempel C, Heneka MT, Hawxhurst V, Fitzgerald ML, Trebicka J, Bjorkhem I, Gustafsson JA, Westerterp M, Tall AR, Wright SD, Espevik T, Schultze JL, Nickenig G, Lutjohann D, Latz E, Cyclodextrin promotes atherosclerosis regression via macrophage reprogramming. Sci. Transl. Med 8, 333ra350 (2016).
48. Del Porto F, Proietta M, di Gioia C, Cifani N, Dito R, Fantozzi C, Ferri L, Fabriani L, Rossi M, Tritapepe L, Taurino M, FGF-23 levels in patients with critical carotid artery stenosis. Intern. Emerg. Med 10, 437–444 (2015). [PubMed: 25573621]
49. Janczak D, Ziolkowski P, Garcarek J, Janczak D Jr., Dorobisz K, Chabowski M, The cytokines within the carotid plaque in symptomatic patients with internal carotid artery stenosis. J. Cardiothorac. Surg 9, 139 (2014).
50. Barrett TJ, Macrophages in Atherosclerosis Regression. Arterioscler. Thromb. Vasc. Biol 40, 20–33 (2020). [PubMed: 31722535]
51. Mahmoud AD, Ballantyne MD, Miscianinov V, Pinel K, Hung J, Scanlon JP, Iyinikkel J, Kaczynski J, Tavares AS, Bradshaw AC, Mills NL, Newby DE, Caporali A, Gould GW, George SJ, Ulitsky I, Sluimer JC, Rodor J, Baker AH, The Human-Specific and Smooth Muscle Cell-Enriched LncRNA SMILR Promotes Proliferation by Regulating Mitotic CENPF mRNA and Drives Cell-Cycle Progression Which Can Be Targeted to Limit Vascular Remodeling. Circ. Res 125, 535–551 (2019). [PubMed: 31339449]
52. Byers PH, Ward PA, Kellermeyer RW, Naff GB, Complement as a mediator of inflammation in acute gouty arthritis. II. Biological activities generated from complement by the interaction of serum complement and sodium urate crystals. J. Lab. Clin. Med 81, 761–769 (1973). [PubMed: 4698661]
53. Fields TR, Abramson SB, Weissmann G, Kaplan AP, Ghebrehiwet B, Activation of the alternative pathway of complement by monosodium urate crystals. Clin. Immunol. Immunopathol 26, 249–257 (1983). [PubMed: 6872344]
54. Portilla D, Xavier S, Role of intracellular complement activation in kidney fibrosis. Br. J. Pharmacol 178, 2880–2891 (2021). [PubMed: 33555070]

55. Niyonzima N, Bakke SS, Gregersen I, Holm S, Sandanger Ø, Orrem HL, Sporsheim B, Ryan L, Kong XY, Dahl TB, Skjelland M, Sørensen KK, Rokstad AM, Yndestad A, Latz E, Gullestad L, Andersen G, Damås JK, Aukrust P, Mollnes TE, Halvorsen B, Espevik T, Cholesterol crystals use complement to increase NLRP3 signaling pathways in coronary and carotid atherosclerosis. EBioMedicine 60, 102985 (2020). [PubMed: 32927275]
56. Reis ES, Mastellos DC, Hajishengallis G, Lambris JD, New insights into the immune functions of complement. Nat. Rev. Immunol 19, 503–516 (2019). [PubMed: 31048789]
57. Smith PK, Shernan SK, Chen JC, Carrier M, Verrier ED, Adams PX, Todaro TG, Muhlbaier LH, Levy JH, Effects of C5 complement inhibitor pexelizumab on outcome in high-risk coronary artery bypass grafting: combined results from the PRIMO-CABG I and II trials. J. Thorac. Cardiovasc. Surg 142, 89–98 (2011). [PubMed: 20880552]
58. Song WC, Crosstalk between complement and toll-like receptors. Toxicol. Pathol 40, 174–182 (2012). [PubMed: 22109714]
59. Haggadone MD, Grailer JJ, Fattahi F, Zetoune FS, Ward PA, Bidirectional Crosstalk between C5a Receptors and the NLRP3 Inflammasome in Macrophages and Monocytes. Mediators Inflamm 2016, 1340156 (2016). [PubMed: 27382187]
60. Sommerfeld O, Medyukhina A, Neugebauer S, Ghait M, Ulferts S, Lupp A, König R, Wetzker R, Schulz S, Figge MT, Bauer M, Press AT, Targeting Complement C5a Receptor 1 for the Treatment of Immunosuppression in Sepsis. Mol. Ther 29, 338–346 (2021). [PubMed: 32966769]
61. Nakano H, Moran TP, Nakano K, Gerrish KE, Bortner CD, Cook DN, Complement receptor C5aR1/CD88 and dipeptidyl peptidase-4/CD26 define distinct hematopoietic lineages of dendritic cells. J. Immunol 194, 3808–3819 (2015). [PubMed: 25769922]
62. Luo C, Chen M, Madden A, Xu H, Expression of complement components and regulators by different subtypes of bone marrow-derived macrophages. Inflammation 35, 1448–1461 (2012). [PubMed: 22450524]
63. Hosszu KK, Santiago-Schwarz F, Peerschke EI, Ghebrehiwet B, Evidence that a C1q/C1qR system regulates monocyte-derived dendritic cell differentiation at the interface of innate and acquired immunity. Innate Immun 16, 115–127 (2010). [PubMed: 19710097]
64. Alpert SE, Auerbach HS, Cole FS, Colten HR, Macrophage maturation: differences in complement secretion by marrow, monocyte, and tissue macrophages detected with an improved hemolytic plaque assay. J. Immunol 130, 102–107 (1983). [PubMed: 6336622]
65. Vijayan V, Pradhan P, Braud L, Fuchs HR, Gueler F, Motterlini R, Foresti R, Immenschuh S, Human and murine macrophages exhibit differential metabolic responses to lipopolysaccharide - A divergent role for glycolysis. Redox Biol 22, 101147 (2019). [PubMed: 30825774]
66. Pelegrin P, Surprenant A, Dynamics of macrophage polarization reveal new mechanism to inhibit IL-1beta release through pyrophosphates. EMBO J 28, 2114–2127 (2009). [PubMed: 19536133]
67. de Gaetano M, Crean D, Barry M, Belton O, M1- and M2-Type Macrophage Responses Are Predictive of Adverse Outcomes in Human Atherosclerosis. Front. Immunol 7, 275 (2016). [PubMed: 27486460]
68. Mandrup-Poulsen T, Immunometabolism in 2017: Metabolism and the inflammasome in health and ageing. Nat. Rev. Endocrinol 14, 72–74 (2018). [PubMed: 29286048]
69. Prochnicki T, Latz E, Inflammasomes on the Crossroads of Innate Immune Recognition and Metabolic Control. Cell Metab 26, 71–93 (2017). [PubMed: 28683296]
70. Roshan MH, Tambo A, Pace NP, The Role of TLR2, TLR4, and TLR9 in the Pathogenesis of Atherosclerosis. Int. J. Inflam 2016, 1532832 (2016). [PubMed: 27795867]
71. Wong YC, Kim S, Peng W, Krainc D, Regulation and Function of Mitochondria-Lysosome Membrane Contact Sites in Cellular Homeostasis. Trends Cell Biol 29, 500–513 (2019). [PubMed: 30898429]
72. Sergin I, Evans TD, Razani B, Degradation and beyond: the macrophage lysosome as a nexus for nutrient sensing and processing in atherosclerosis. Curr. Opin. Lipidol 26, 394–404 (2015). [PubMed: 26241101]
73. Ghebrehiwet B, Hosszu KH, Peerschke EI, C1q as an autocrine and paracrine regulator of cellular functions. Mol. Immunol 84, 26–33 (2017). [PubMed: 27914690]

74. Son M, Porat A, He M, Suurmond J, Santiago-Schwarz F, Andersson U, Coleman TR, Volpe BT, Tracey KJ, Al-Abed Y, Diamond B, C1q and HMGB1 reciprocally regulate human macrophage polarization. Blood 128, 2218–2228 (2016). [PubMed: 27683415]
75. Thielens NM, Tedesco F, Bohlson SS, Gaboriaud C, Tenner AJ, C1q: A fresh look upon an old molecule. Mol. Immunol 89, 73–83 (2017). [PubMed: 28601358]
76. Wu B, Luo H, Zhou X, Cheng CY, Lin L, Liu BL, Liu K, Li P, Yang H, Succinate-induced neuronal mitochondrial fission and hexokinase II malfunction in ischemic stroke: Therapeutical effects of kaempferol. Biochim. Biophys. Acta Mol. Basis. Dis 1863, 2307–2318 (2017). [PubMed: 28634116]
77. Robey RB, Hay N, Mitochondrial hexokinases, novel mediators of the antiapoptotic effects of growth factors and Akt. Oncogene 25, 4683–4696 (2006). [PubMed: 16892082]
78. Roberts DJ, Miyamoto S, Hexokinase II integrates energy metabolism and cellular protection: Akting on mitochondria and TORCing to autophagy. Cell Death Differ 22, 248–257 (2015). [PubMed: 25323588]
79. Tam JC, Bidgood SR, McEwan WA, James LC, Intracellular sensing of complement C3 activates cell autonomous immunity. Science 345, 1256070 (2014). [PubMed: 25190799]
80. Brott TG, Halperin JL, Abbara S, Bacharach JM, Barr JD, Bush RL, Cates CU, Creager MA, Fowler SB, Friday G, Hertzberg VS, McIff EB, Moore WS, Panagos PD, Riles TS, Rosenwasser RH, Taylor AJ, 2011 ASA/ACCF/AHA/AANN/AANS/ACR/ASNR/CNS/SAIP/SCAI/SIR/SNIS/SVM/SVS guideline on the management of patients with extracranial carotid and vertebral artery disease: executive summary. J. Neurointerv. Surg 3, 100–130 (2011). [PubMed: 21990803]
81. Wieckowski MR, Giorgi C, Lebiedzinska M, Duszynski J, Pinton P, Isolation of mitochondria-associated membranes and mitochondria from animal tissues and cells. Nat. Protoc 4, 1582–1590 (2009). [PubMed: 19816421]
82. Zhang J, Woodruff TM, Clark RJ, Martin DJ, Minchin RF, Release of bioactive peptides from polyurethane films in vitro and in vivo: Effect of polymer composition. Acta Biomater 41, 264–272 (2016) [PubMed: 27245428]
83. Kumar V, Lee JD, Clark RJ, Noakes PG, Taylor SM, Woodruff TM, Preclinical Pharmacokinetics of Complement C5a Receptor Antagonists PMX53 and PMX205 in Mice. ACS Omega 5, 2345–2354 (2020). [PubMed: 32064396]
84. Rousset X, Vaisman B, Auerbach B, Krause BR, Homan R, Stonik J, Csako G, Shamburek R, Remaley AT, Effect of recombinant human lecithin cholesterol acyltransferase infusion on lipoprotein metabolism in mice. J. Pharmacol. Exp. Ther 335, 140–148 (2010). [PubMed: 20605907]
85. Li B, Dewey CN, RSEM: accurate transcript quantification from RNA-Seq data with or without a reference genome. BMC Bioinform 12, 323 (2011).
86. Robinson MD, McCarthy DJ, Smyth GK, edgeR: a Bioconductor package for differential expression analysis of digital gene expression data. Bioinformatics 26, 139–140 (2010). [PubMed: 19910308]
87. Subramanian A, Tamayo P, Mootha VK, Mukherjee S, Ebert BL, Gillette MA, Paulovich A, Pomeroy SL, Golub TR, Lander ES, Mesirov JP, Gene set enrichment analysis: a knowledge-based approach for interpreting genome-wide expression profiles. Proc. Natl. Acad. Sci. U S A 102, 15545–15550 (2005). [PubMed: 16199517]
88. Dobin A, Davis CA, Schlesinger F, Drenkow J, Zaleski C, Jha S, Batut P, Chaisson M, Gingeras TR, STAR: ultrafast universal RNA-seq aligner. Bioinformatics 29, 15–21 (2013). [PubMed: 23104886]
89. Liao Y, Smyth GK, Shi W, featureCounts: an efficient general purpose program for assigning sequence reads to genomic features. Bioinformatics 30, 923–930 (2014). [PubMed: 24227677]

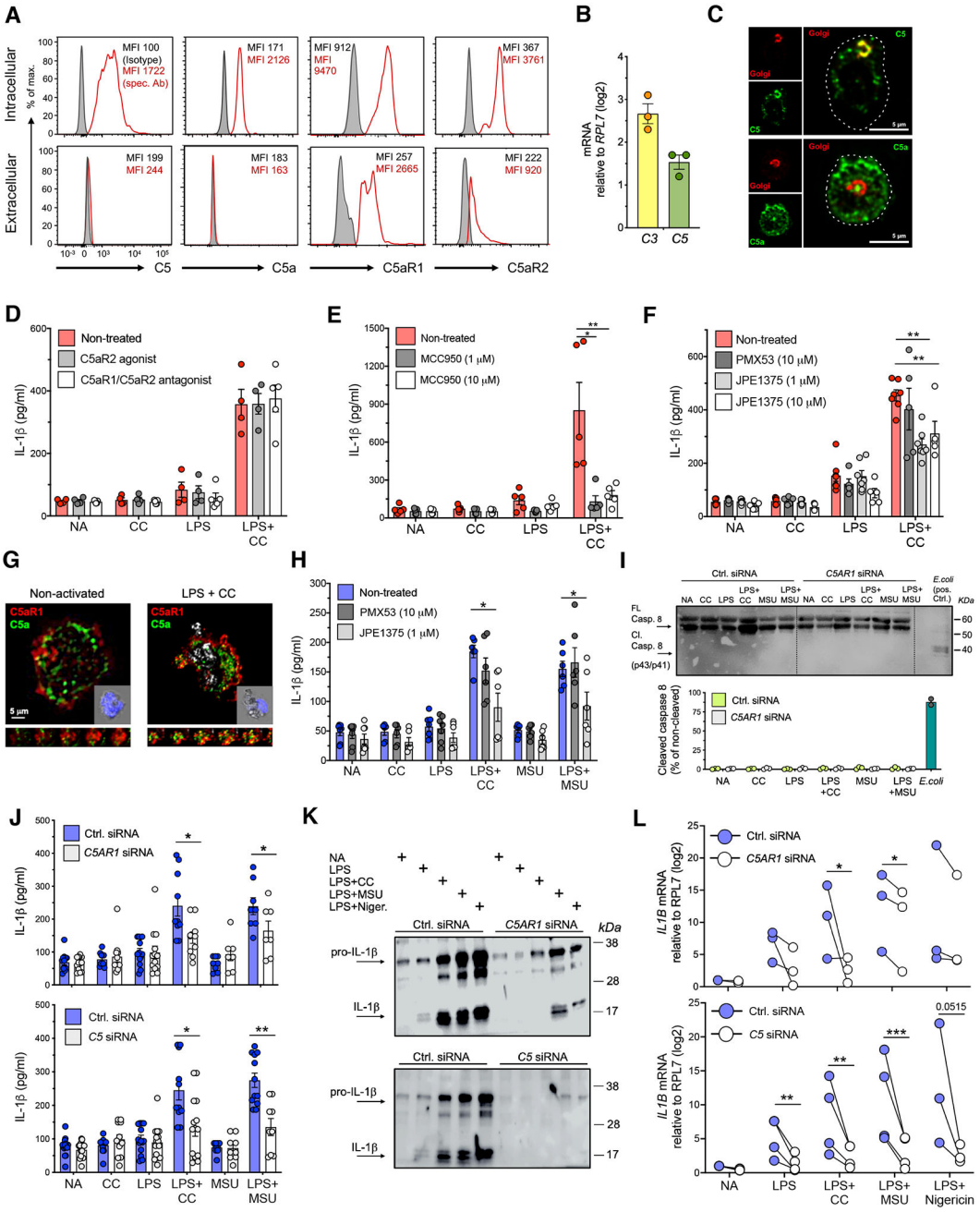

Fig. 1. Intracellular C5aR1 supports IL-1β production in crystal-sensing monocytes and macrophages.

(**A**) Assessment of resting human monocytes for intracellular C5 and C5a and C5aR1 and C5aR2 expression by flow cytometry (representative result of n=5). (**B** and **C**) *C5* gene expression (**B**) and C5 protein presence in the Golgi apparatus (**C**) denote cell-intrinsic C5 generation (both representative of n=3 donors). (**D** to **F**) IL-1β production by human monocytes pretreated with extracellular C5aR2 agonist or C5aR1/C5aR2 antagonist (**D**), the NLRP3 inflammasome inhibitor MCC950 (**E**) or C5aR1 antagonist PMX53 (low cell-permeability) or C5aR1 antagonist JPE1375 (high cell-permeability) (**F**) prior

to LPS priming (2 hrs) and CC exposure for 14 hrs (n=5–8). (**G**) C5a and C5aR1 colocalization in resting and LPS+CC-activated (6 hrs) monocytes assessed via confocal microscopy (detection of CC by light microscopy inserted) and Z-stack analysis (lower panels) (representative of n=5, original magnification 100 x). (**H**) Impact of extracellular (PMX53) or extra- and intracellular (JPE1375) C5aR1 inhibition on IL-1β secretion by LPS+CC-activated human macrophages (n=4–6). (**I**) Effect of C5aR1 silencing in human primed and/or crystal-activated macrophages on active caspase-8 generation (n=3). Cells were exposed to *E. coli* for 24 hrs as positive control. (**J**) Effect of C5aR1 (upper panels) or C5 (lower panels) knock-down via siRNA technique on IL-1β secretion by CC or MSU crystal-activated THP-1 cells (n=7–14). (**K** and **L**) Impact of C5aR1 (upper panel) or C5 (lower panel) knock-down on IL-1β pro- vs. mature protein levels (**K**) and *IL1B* gene transcription (**L**) by CC, MSU crystal or nigericin-activated THP-1 cells (n=3). Error bars in graphs represent mean ± SEM. (D–F), (J), two-way ANOVA with Bonferroni's post-test; (H), (L), Wilcoxon matched-paired signed rank tests. *p <0.05, **p <0.01, ***p <0.005.

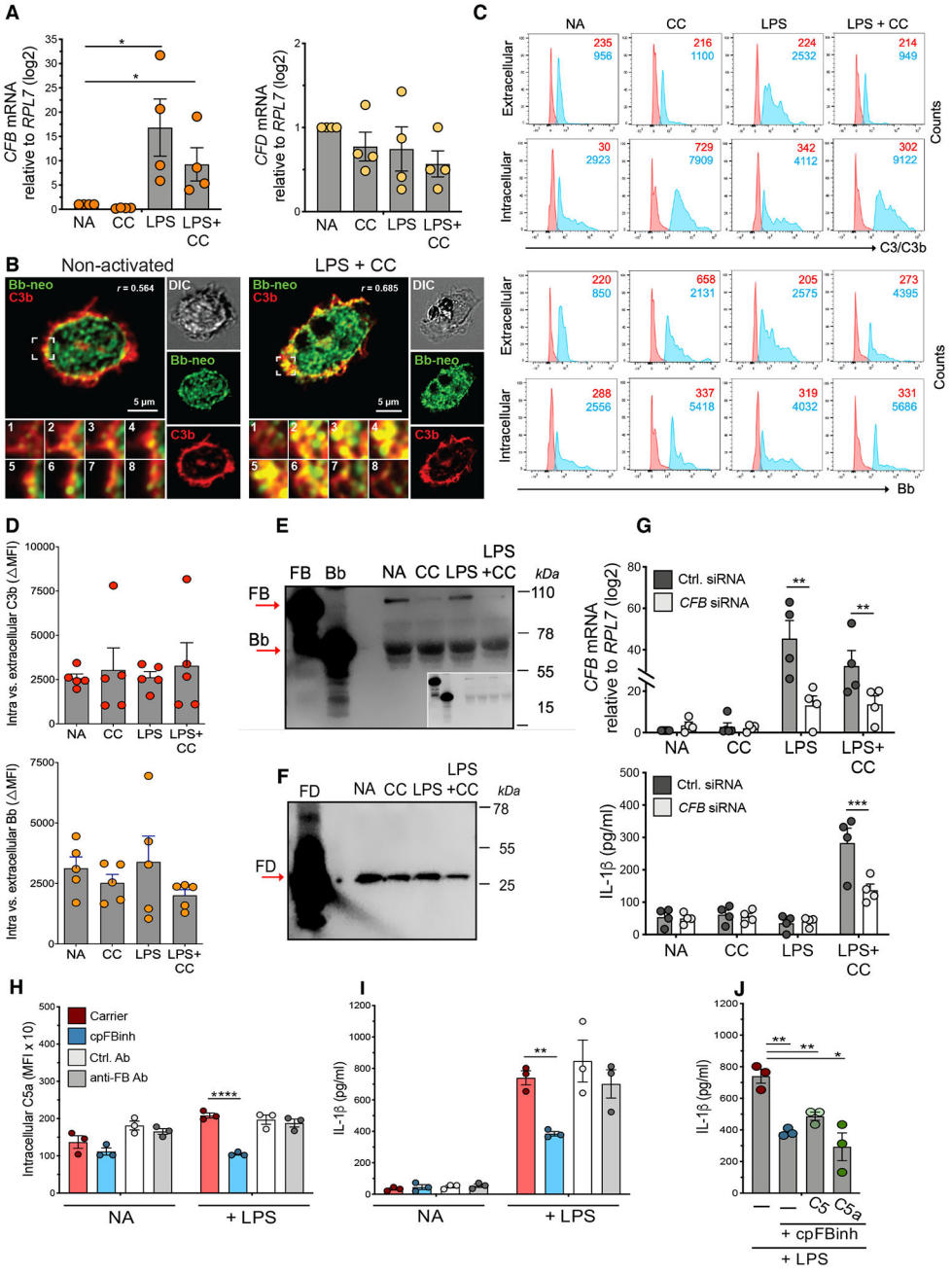

Fig. 2. An intracellular C5 convertase drives C5a generation within CC-sensing monocytes.

(**A**) Effect of TLR4 priming on *CFB* (left panel) and *CFD* (right panel) gene expression in non-activated (NA) or CC-activated (4 hrs) human monocytes (n=4). (**B**) Detection of intracellular C3/C5 convertase generation (C3bBb, and/or C3bBbC3b) by confocal microscopy in non-activated or LPS+CC-timulated monocytes (representative of n=3). (**C** and **D)** Measurement of extra- vs. intracellular C3b (upper panel) and Bb (activated FB, lower panel) protein amounts in resting and activated monocytes 4 hrs post activation. Representative FACS plot (**C**) and combined data plotted (**D**) (n=4). **(E** and **F**) Assessment of activated and resting monocytes for active (Bb) and non-active FB (**E**) or for FD (**F**,

data shown are representative of n=2). (**G**) Impact of *CFB* expression knock-down via siRNA (**upper panel**) on IL-1β production by primed and/or CC-exposed macrophages **(lower panel)** (n=4). (**H** and **I**) Impact of intra- or extracellular C3 convertase inhibition on monocyte cell-intrinsic C5a generation and IL-1β production. Human monocytes were left non-activated or were activated with LPS (100 ng/ml) after pre-incubation with or without a cell-permeable FB inhibitor (cpFBinh) or anti-FB antibody (Ab) or carrier or control (Ctrl.) Ab and intracellular C5a assessed by flow cytometry (**H**) and IL-1β (**I**) secretion measured at 4 hrs post activation (n=3). (**J**) Effects of exogenous C5 or C5a supplementation on IL-1β production by cpFBinh-treated monocytes *in vitro*. Monocytes were activated in the presence of cpFBinh w/wo C5 or C5a supplementation and IL-1β measured 8 hrs post activation (n=3). and Error bars in graphs represent mean ± SEM. (A), (J), one-way ANOVA; (G–I), two-way ANOVA with Bonferroni's post-test. *p <0.05, **p <0.01.

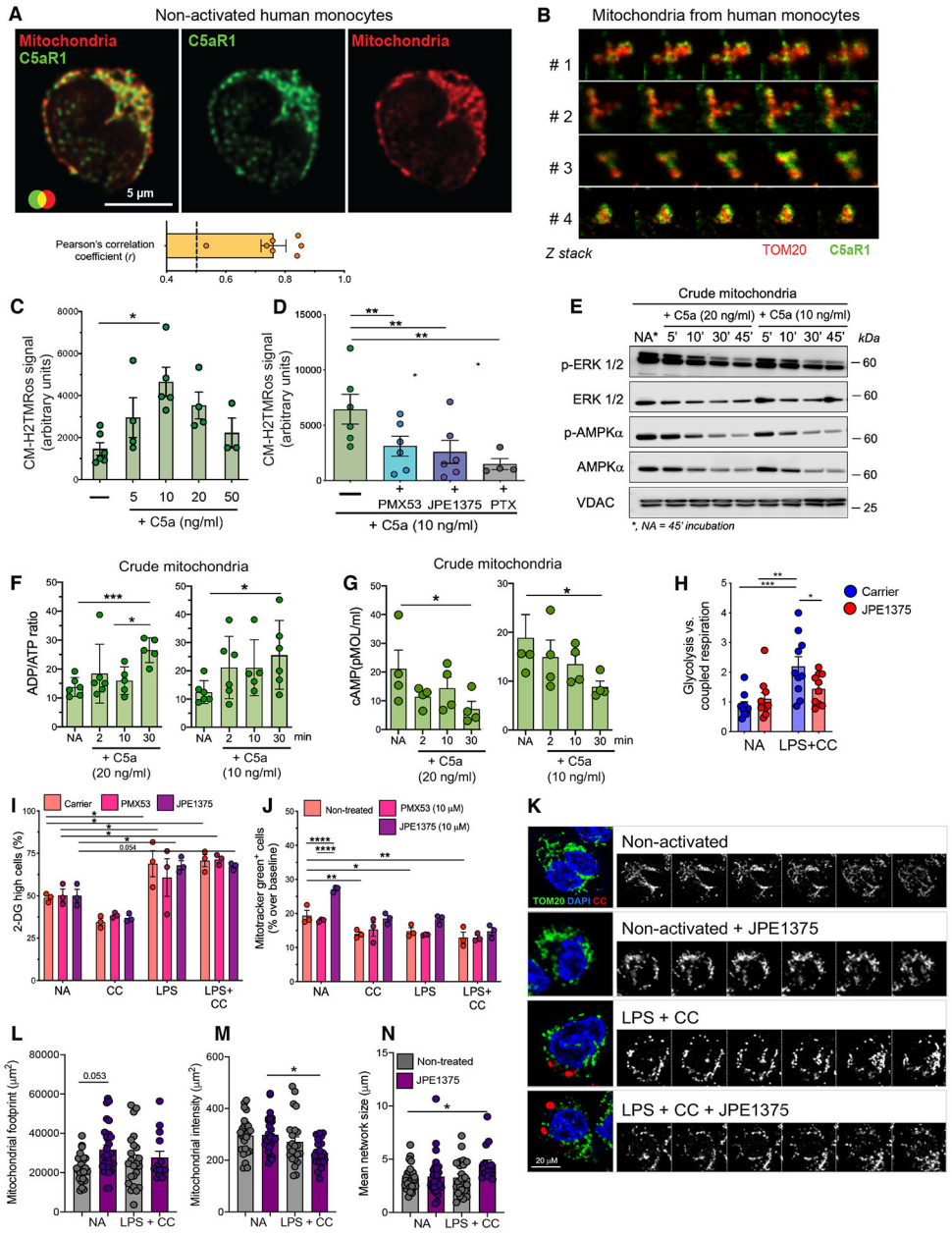

Fig. 3. Mitochondrial C5aR1 controls ETC flux and mitochondrial dynamics.

(**A**) Staining of monocytes for mitochondria and C5aR1, upper panel, and Pearson's correlation coefficient for mitochondria-C5aR1 colocalization, lower panel (n=7, original magnification 100 x). (**B**) Confocal microscopy assessment of C5aR1 and TOM20 expression on mitochondria isolated from human monocytes. Data are presented as Z-stack analysis (n=4). (**C** and **D**) ROS production by isolated mitochondria after stimulation with different amounts of C5a (**C**, n=4) or with 10 ng/ ml C5a in the absence or presence of PMX53, JPE1375, or pertussis toxin (PTX) pre-incubation (**D**, n=4–6). (**E**) Impact of C5a on ERK1/2 and AMPK-α phosphorylation in isolated mitochondria assessed by Western blotting (control VDAC) (data representative of n=4–5 independent experiments). (**F** and **G**) Effect of C5a on purified mitochondrial ADP/ATP balance (**F**) and cAMP production

(**G**) at indicated time points post C5a exposure (n=4–5). (**H**) Effect of intracellular C5aR1 inhibition on glycolysis (ECAR) versus ATP-coupled respiration in LPS+CC-activated human monocytes measured at 4 hrs post activation by Seahorse analysis (n=11). (**I**) Effect of extra- or intracellular C5aR1 inhibition on 2-DG uptake of monocytes after priming and/or CC-sensing (n=3). (**J**) Mitochondrial mass in resting and activated monocytes with or without PMX53 or JPE1375 pre-incubation (n=3). (**L** to **N**) Mitochondrial dynamics in CC-sensing THP-1 cells with or without JPE1375 treatment. Shown is a representative image of cells stained with TOM20 and Z-stacks analysis of each treatment condition (**K**) and analysis of mitochondrial footprint (**L**), intensity (**M**), and mean network size (**N**) (n=15–38). Error bars in graphs represent mean ± SEM. (C), unpaired *t* tests; (D), (H), (I), (J), (L–N), two-way ANOVA with Bonferroni's post-test; (F), (G), one-way ANOVA. *p <0.05, **p <0.01, ***p <0.005, ****p <0.001.

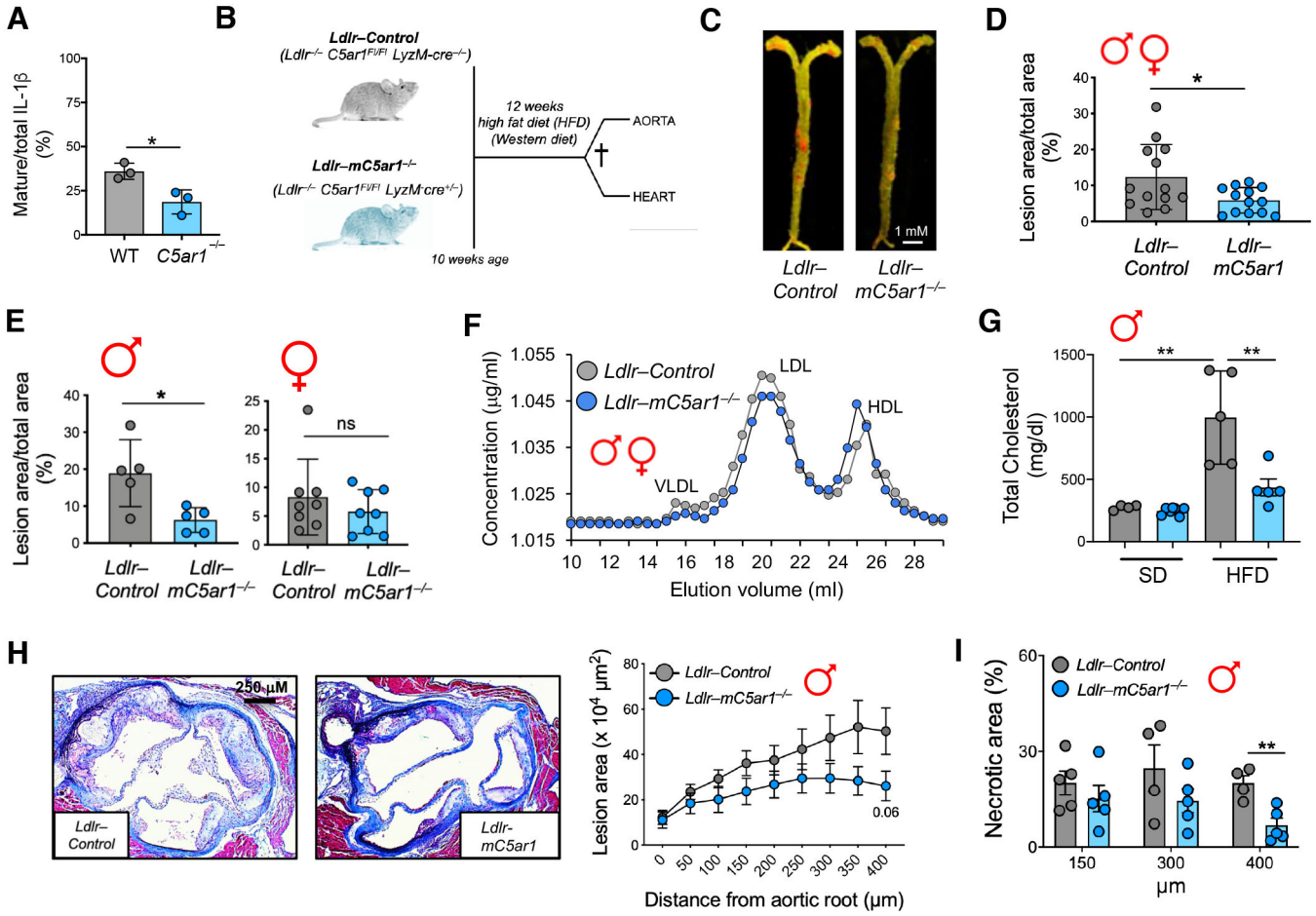

Fig. 4. High fat diet-induced atherosclerosis is driven by macrophage-expressed C5aR1.

(**A**) Mature IL-1β generation of BMDMs from wild type (WT) or global *C5ar1*$^{-/-}$ mice at 12 hrs post activation with LPS+CC (n=3). (**B**) Schematic of the high fat (cholesterol or Western) diet-induced atherosclerosis mouse model and animals (*Ldlr*- and myeloid *C5ar1*-deficient mice, *Ldlr–mC5ar1*$^{-/-}$; *Ldlr*$^{-/-}$ *C5ar1*$^{Fl/Fl}$ *LyzM-cre*$^{+/-}$) and control mice (*Ldlr*$^{-/-}$ *C5ar1*$^{Fl/Fl}$ *LyzM-cre*$^{-/-}$) utilized. (**C**) Representative image of the entire aorta isolated from a male control or male *Ldlr–mC5ar1*$^{-/-}$ mouse with plaques visualized by Sudan IV staining (original magnification 0.5 x). (**D** and **E**) Quantification of aortic lesions of all mice (**D**, n=13) and of mice separated by sex (**E**, male=5; female=8). (**F**) Circulating LDL, VLDL, and HDL in control and *Ldlr–mC5aR1*$^{-/-}$ mice (mix of male and female animals, pooled plasma, n=7/group) before transfer to a HFD. (**G**) Total cholesterol levels in male control and *Ldlr–mC5ar1*$^{-/-}$ mice at 12 weeks on either a standard diet (SD) or high fat die (HFD) (n=5). (**H**) Heart aortic root plaque size in male control and *Ldlr–mC5ar1*$^{-/-}$ mice (left panel, representative image (n=5); original magnification, 50 x) and quantification of lesion area (right panel). **(I)** Necrotic area formation through the heart aortic root at indicated depths. (D), (E), unpaired *t* tests; (G–I), two-way ANOVA. Error bars in graphs represent mean ± SEM. **p* <0.05, ***p* <0.01.

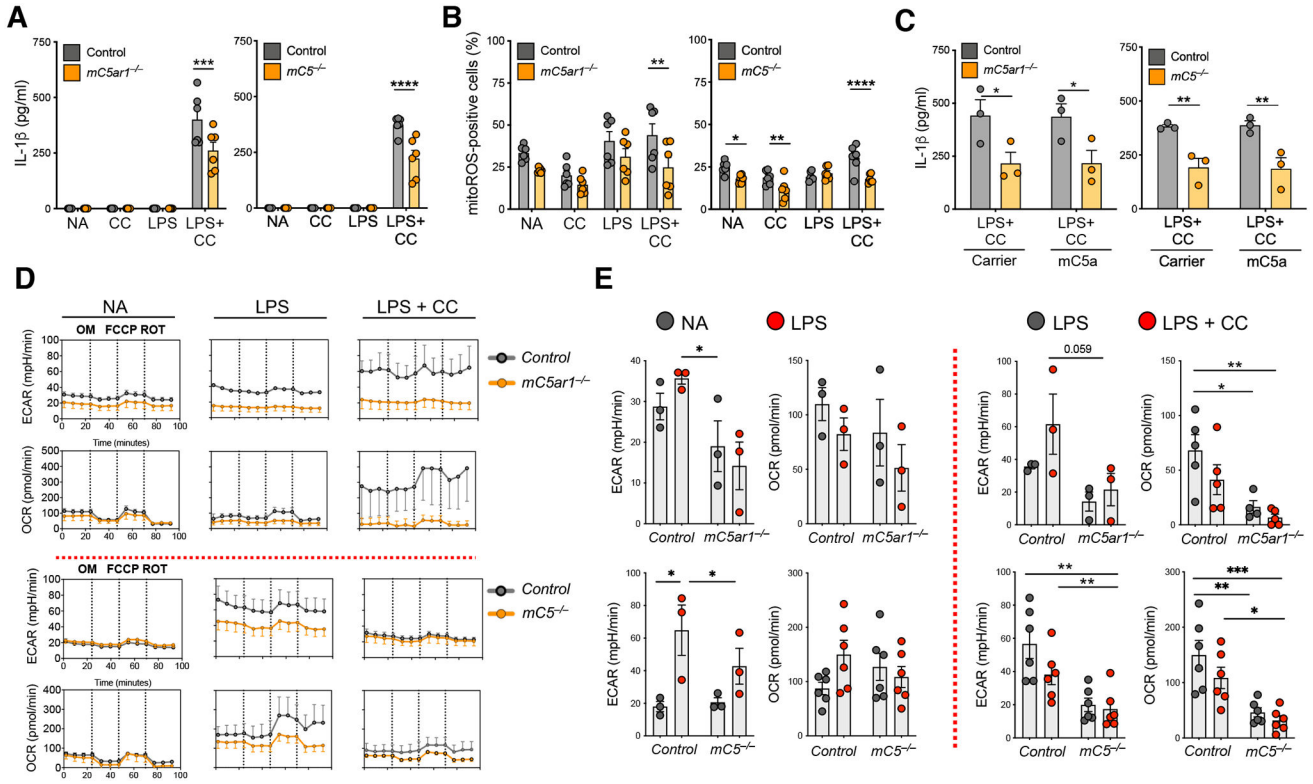

Figure 5. Cell-autonomous C5 drives metabolic adaption and IL-1β secretion upon crystal-sensing.

(**A** and **B**) IL-1β secretion (**A**) and mitochondrial ROS production (**B**) by BMDMs from male and female *mC5ar1*$^{-/-}$ (left panels) or *mC5*$^{-/-}$ (right panels) mice after priming with LPS (4 hrs) and subsequent exposure to CC (4 hrs) (n=6). (**C**) Effect of C5a supplementation into media on IL-1β production from *mC5ar1*$^{-/-}$ (left panels) or *mC5*$^{-/-}$ primed BMDMs upon crystal-sensing (n=3, activation performed as under '**A**'). (**D** and **E**) Impact of *C5ar1* or *C5* deficiency on glycolysis (ECAR) and OXPHOS (OCR) in BMDMs upon LPS priming and CC sensing. Representative seahorse profile (**D**) with summarized data (**E**, n=3–6). Error bars in graphs represent mean ± SEM. (A), (B), (E), two-way ANOVA with Bonferroni's post-test; (C), unpaired *t* tests. **p* <0.05, ***p* <0.01, ****p* <0.001, *****p* <0.0001.

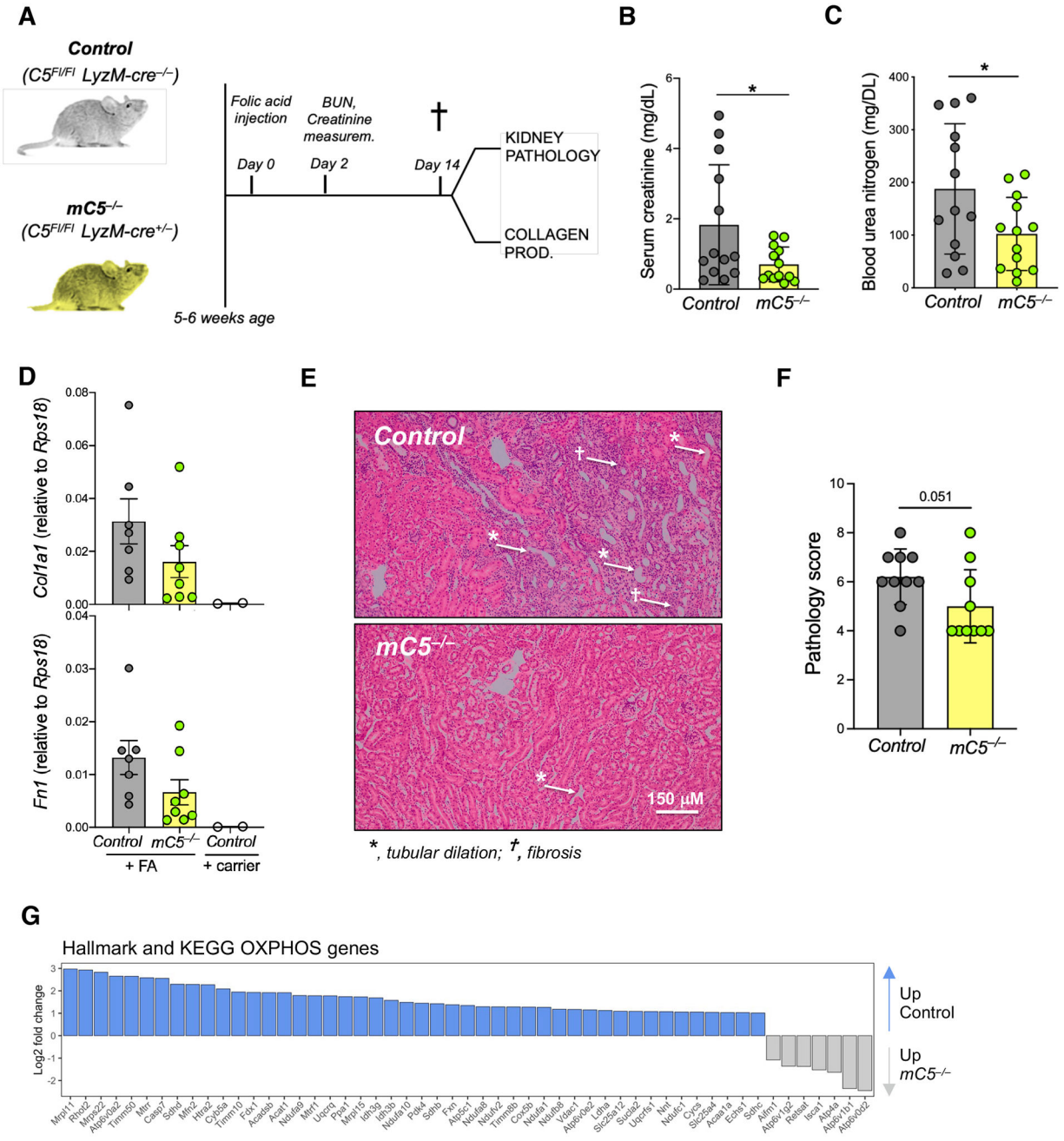

Figure 6. Macrophage intracellular C5aR1 activity drives pathology in AKI.

(**A**) Depiction of the folic acid (FA)-induced acute kidney injury (AKI) model used. (**B** and **C**) Measurement of serum creatinine (**B**) and blood urea nitrogen (BUN) (**C**) in mice measured at day 2 post FA injection (n=12–13). (**D**) PCR analysis of collagen (*Col1a1*) and fibronectin (*Fn1*) mRNA in kidney tissue samples from mice scarified at day 14 post FA injection (n=7–9). (**E** and **F**) Histopathological analysis of kidney biopsies (day 14) with a representative H&E staining (**E**, original magnification 10 x) and summarized injury scores (n=7–10) (**F**). (**G**) Barplot showing log2 fold changes of genes involved in oxidative phosphorylation (OXPHOS) when comparing kidney-derived wild type control or *C5*$^{-/-}$

monocytes following FA-induced AKI. OXPHOS genes were taken from Hallmark and KEGG collections, and only genes with a log2 fold change > 1 are shown. Error bars in graphs represent mean ± SEM. (B), (C), (F), unpaired *t* tests. **p* <0.05.

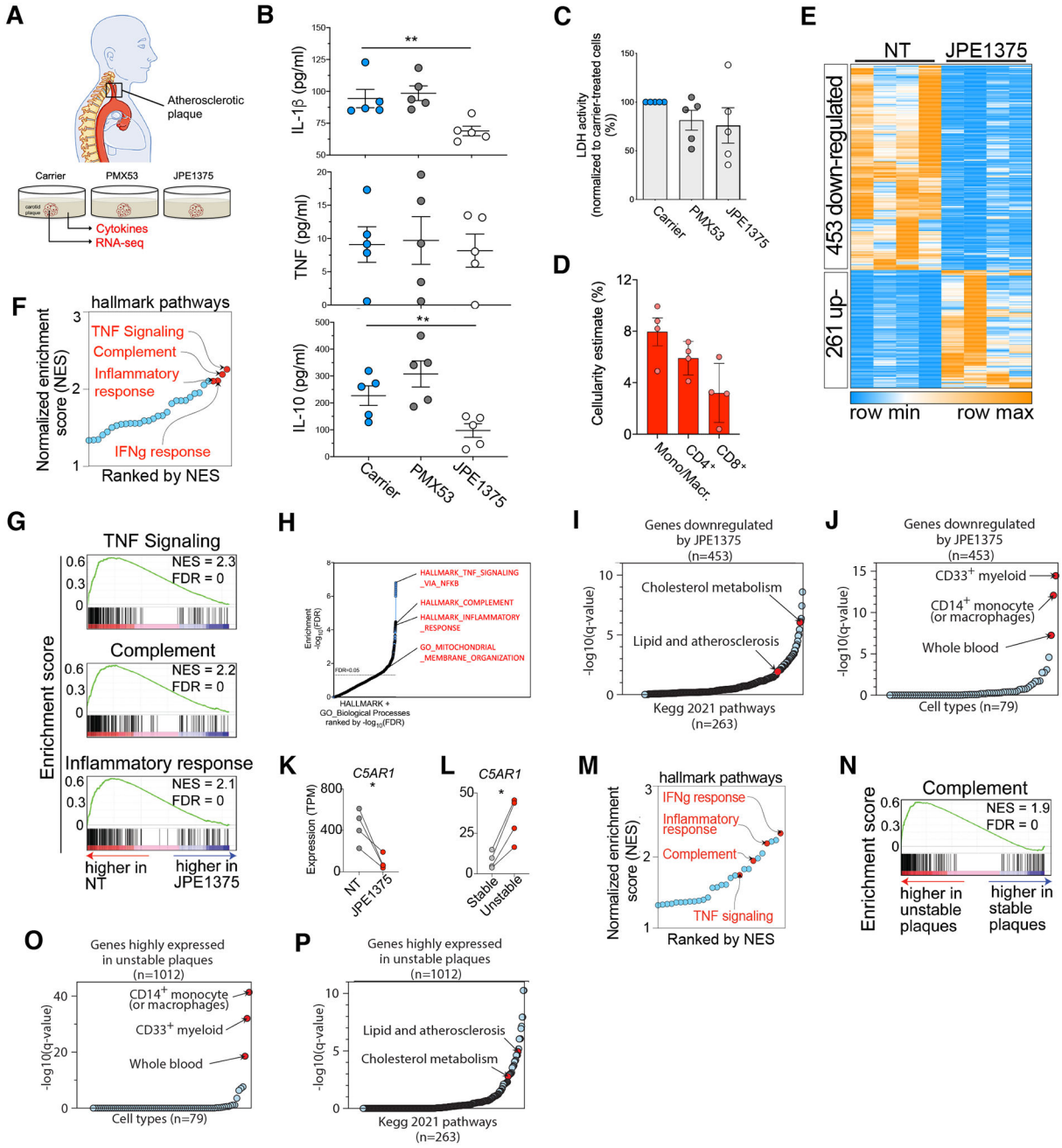

Fig. 7. Intracellular C5aR1 inhibition attenuates the inflammatory milieu of carotid plaques.

(**A**) *Ex vivo* system for examining effects of extracellular (PMX53) or extra- and intracellular (JPE1375) C5aR1 inhibition on the carotid plaque inflammatory 'state'. Human atherosclerotic carotid plaques were obtained by carotid endarterectomy (n=5), separated into macroscopically equal pieces and cultured with either PMX53, JPE1375 or a carrier solution (16 hrs). Cell supernatants were analyzed for cytokines and cells used for RNA-sequencing analysis. (**B**) Effect of C5aR1 inhibition on IL-1β, TNF and IL-10 production (n=5) and (**C**) on cell viability. (**D**) Macrophage and T cell composition of plaques as assessed from gene expression signatures (**E**) (n=4). (**E**) Assessment of genes in plaque-

resident cells affected by JPE1375 treatment. (**F**) Hallmark immune pathways enriched in carrier-treated plaques (false discovery rate (FDR) < 0.05) by gene set enrichment analysis (GSEA) compared to JPE1375-treated plaques. Pathways are ranked by normalized enrichment score; highlighted are top 4 pathways in red. (**G**) Representative GSEA plots showing top ranked pathways from (**E**). (**H** and **I**) Hallmark and GO (**H**) and Kegg (**I**) pathways enriched in 453 genes downregulated in plaques after treatment with JPE1375. The select pathways are highlighted. Pathways are ranked by FDR. (**J**) Enrichment of marker genes from 79 known immune cell types within 453 genes downregulated in plaques after JPE1375 treatment. (**K** and **L**) *C5AR1* mRNA expression in JPE1375-treated versus non-treated (NT) plaques (**K**) and stable versus unstable plaques (**L**) (n=4). (**M** and **N**) Hallmark pathways enriched in unstable plaques (FDR < 0.05) by GSEA compared to stable plaques (**M**) with specific assessment of the complement pathway (**N**). (**O**) Enrichment of marker genes from 79 known immune cell types within 1012 genes highly expressed in unstable plaques compared to stable plaques. (**P**) Kegg pathways enriched in 1012 genes highly expressed in unstable plaques compared to stable plaques. Select top metabolic pathways are highlighted. Error bars in graphs represent mean ± SEM. (B), one-way ANOVA; (K), (L), paired *t* tests. *p <0.05, **p <0.01

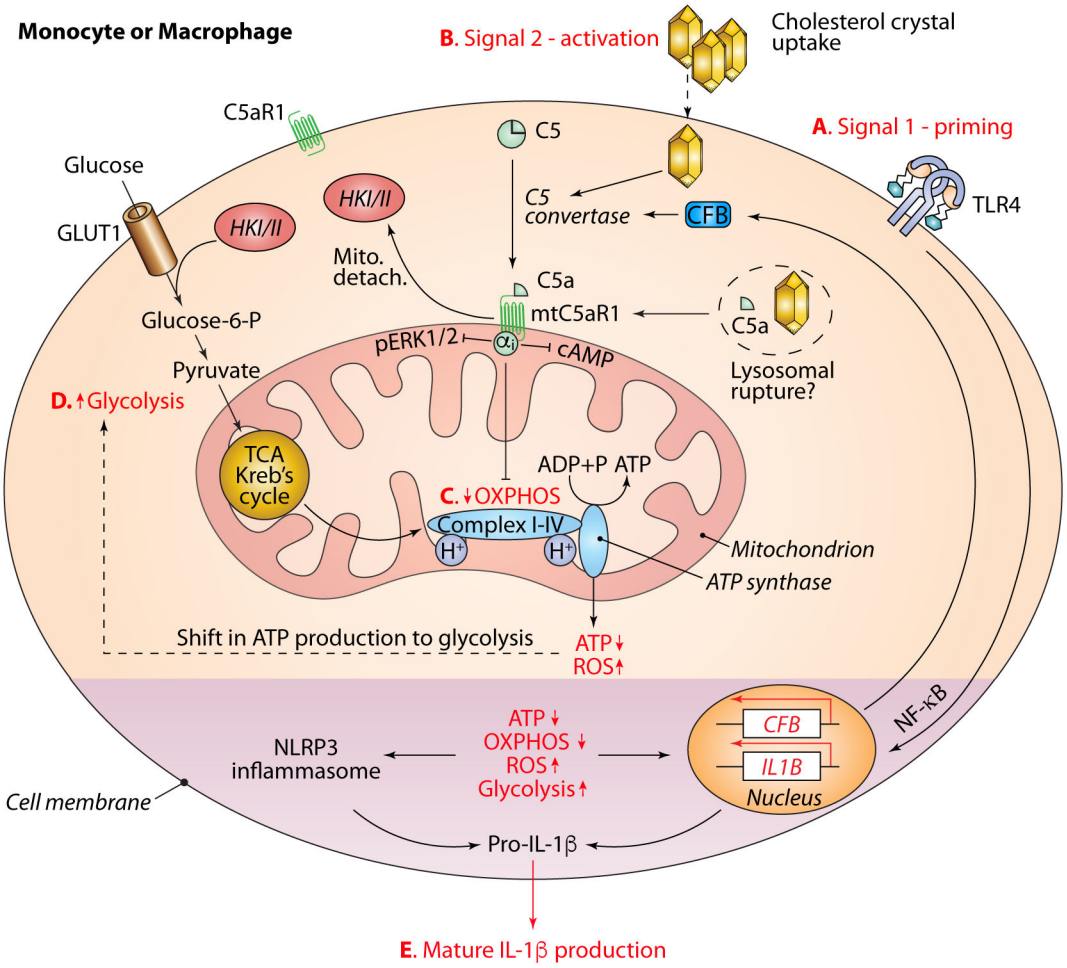

Figure 8. MtC5aR1 contributions to IL-1β production upon CC-sensing.

Monocytes and macrophages express the C5aR1 constitutively on mitochondria (mtC5aR1) and continuously generate intracellular C5a via an intracellular C5 convertase. TLR4 engagement by endogenous danger signals (for example, modified LDLs) triggers a priming Signal 1 (A) that induces (increased) transcription of the *IL1B* and *CFB* genes. Uptake of CC amplifies cell-intrinsic C5a production by augmented C5 convertase formation and triggers mtC5aR1 ligation (B). MtC5aR1 activation, in a G protein-coupled fashion (α_i), reduces mitochondrial ERK1/2 phosphorylation, ATP and cAMP formation, and OXPHOS (C) and simultaneously increases ROS production and glycolysis (D) via reverse electron transport and also induces detachment of HKI from mitochondria. Together, these events further elevate *IL1B* gene transcription and also provide Signal 2 (B) for the assembly of the NLRP3 inflammasome and processing of immature pro-IL1β into mature IL-1β (E). (?), hypothetical provision of C5a to mtC5aR1 via CC-induced lysosomal rupture. ATP, adenosine triphosphate; cAMP, cyclic adenosine monophosphate; CC, cholesterol crystals; GLUT1, glucose transporter 1; HKI/II, hexokinase I (or II); OXPHOS, oxidative phosphorylation; ROS, reactive oxygen species.